

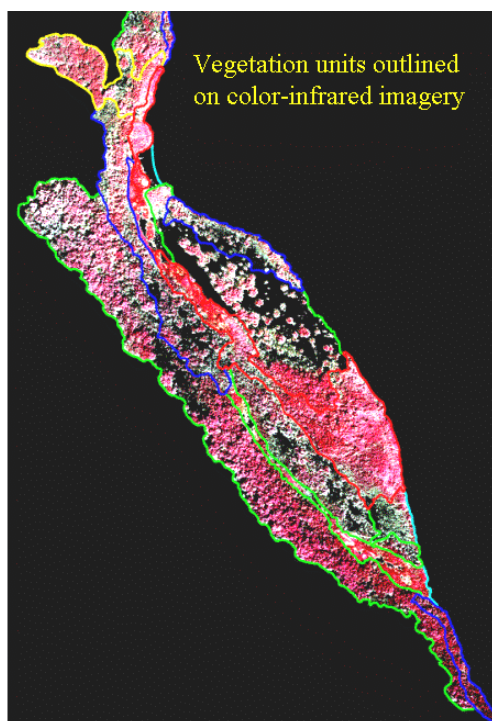


Evaluation of airborne image data for mapping riparian vegetation within the Grand Canyon

by Philip A. Davis¹
Matthew I. Staid¹,
Jeffrey B. Plescia¹,
and Jeffrey R. Johnson¹

Open-File Report 02-470

2002



This report is preliminary and has not been reviewed for conformity with U.S. Geological Survey editorial standards or with the North American Stratigraphic Code. Any use of trade, firm, or product names is for descriptive purposes only and does not imply endorsement by the U.S. Government.

U.S. DEPARTMENT OF THE INTERIOR
U.S. GEOLOGICAL SURVEY

¹Flagstaff, Arizona

Abstract

This study examined various types of remote-sensing data that have been acquired during a 12-month period over a portion of the Colorado River corridor to determine the type of data and conditions for data acquisition that provide the optimum classification results for mapping riparian vegetation. Issues related to vegetation mapping included time of year, number and positions of wavelength bands, and spatial resolution for data acquisition to produce accurate vegetation maps versus cost of data. Image data considered in the study consisted of scanned color-infrared (CIR) film, digital CIR, and digital multispectral data, whose resolutions from 11 cm (photographic film) to 100 cm (multispectral), that were acquired during the Spring, Summer, and Fall seasons in 2000 for five long-term monitoring sites containing riparian vegetation. Results show that digitally acquired data produce higher and more consistent classification accuracies for mapping vegetation units than do film products. The highest accuracies were obtained from nine-band multispectral data; however, a four-band subset of these data, that did not include short-wave infrared bands, produced comparable mapping results. The four-band subset consisted of the wavelength bands 0.52-0.59 μm , 0.59-0.62 μm , 0.67-0.72 μm , and 0.73-0.85 μm . Use of only three of these bands that simulate digital CIR sensors produced accuracies for several vegetation units that were 10% lower than those obtained using the full multispectral data set. Classification tests using band ratios produced lower accuracies than those using band reflectance for scanned film data; a result attributed to the relatively poor radiometric fidelity maintained by the film scanning process, whereas calibrated multispectral data produced similar classification accuracies using band reflectance and band ratios. This suggests that the intrinsic band reflectance of the vegetation is more important than inter-band reflectance differences in attaining high mapping accuracies. These results also indicate that radiometrically calibrated sensors that record a wide range of radiance produce superior results and that such sensors should be used for monitoring purposes.

When texture (spatial variance) at near-infrared wavelength is combined with spectral data in classification, accuracy increased most markedly (20-30%) for the highest resolution (11-cm) CIR film data, but decreased in its effect on accuracy in lower-resolution multi-spectral image data; a result observed in previous studies (Franklin and McDermid 1993, Franklin et al. 2000, 2001). While many classification unit accuracies obtained from the 11-cm film CIR band with texture data were in fact higher than those produced using the 100-cm, nine-band multispectral data with texture, the 11-cm film CIR data produced much lower accuracies than the 100-cm multispectral data for the more sparsely populated vegetation units due to saturation of picture elements during the film scanning process in vegetation units with a high proportion of alluvium. Overall classification accuracies obtained from spectral band and texture data range from 36% to 78% for all databases considered, from 57% to 71% for the 11-cm film CIR data, and from 54% to 78% for the 100-cm multispectral data. Classification results obtained from 20-cm film CIR band and texture data, which were produced by applying a Gaussian filter to the 11-cm film CIR data, showed increases in accuracy due to texture that were similar to those observed using the original 11-cm film CIR data. This suggests that data can be collected at the lower resolution and still retain the added power of vegetation texture. Classification accuracies for the riparian vegetation units examined in this study do not appear to be influenced by season of data acquisition, although data acquired under direct sunlight produced higher overall accuracies than data acquired under overcast conditions. The latter observation, in addition to the importance of band reflectance for classification, implies that data should be acquired near summer solstice when sun elevation and reflectance is highest and when shadows cast by steep canyon walls are minimized.

Introduction

The Grand Canyon Monitoring and Research Center (GCMRC) of the U.S. Geological Survey studies the effects of water release from Glen Canyon Dam (operational in 1964) on the resources of the Colorado River within the Grand Canyon (from Lake Powell to Lake Mead) in order to develop release protocols that minimize adverse effects on river ecology. These studies began in 1983, originally under the Glen Canyon Environmental Studies group. The GCMRC is concerned with monitoring and preservation issues related to (1) terrestrial vegetation habitats; (2) aquatic food base and habitats; (3) sediment movement and storage (within the river channel and along the shore); and (4) cultural resources (e.g., archaeological and historic monuments, springs, and mineral deposits). The monitoring program has relied mostly on in-situ measurements, supplemented by annual acquisition of black-and-white or natural-color aerial photographic products. With the exception of photogrammetric analyses, use of these remote-sensing data have been limited to visual interpretation and mapping of surface features using unrectified prints, followed by the transference of the interpretations into a GIS environment. This approach is error prone because (1) the amount of information shown on the photographic prints is less than the true spatial resolution of the film data and very much dependent on the photographic duplication process and (2) the transference of interpretative information to digital, rectified format adds another level of positional uncertainty. Digital data formats (either scanned film or direct digital acquisition) lessen (in the case of scanned film) or eliminate (using digital cameras) these problems and provide databases that can be used directly in image processing or GIS environments, thus allowing more accurate, rigorous, and timely data analyses. The river corridor monitored by GCMRC extends for more than 450 km and, therefore, cost for digital data (which may include multiple wavelength bands at high spatial resolution) is a major concern.

In the Fall 1999, GCMRC started a remote-sensing initiative to study the capabilities and cost-benefits of various types of multiple-wavelength remote-sensing data acquired at different spatial resolutions and in different seasons, specifically for achieving monitoring program objectives. The primary objective of the first phase of the remote-sensing initiative was to identify candidate remote-sensing instruments that satisfy GCMRC program-monitoring requirements. During the year 2000, the selected suite of sensors was used to collect image data for various portions of the Colorado River. This report summarizes the results of our examination of each of the collected remote-sensing databases to identify the data that provides the most cost-effective, accurate means for mapping riparian vegetation types and habitats. Although remote sensing methods may never completely replace in-situ measurements, they have been shown in many instances to provide a cost-effective means of mapping large areas and to reduce the time and expense of field surveys, which in turn may allow expanded monitoring of the environment. We examined the several image databases to address three issues for riparian mapping within the Grand Canyon: (1) data characteristics (number and wavelength of bands, spatial resolution, radiometric fidelity, texture) that provide reliable mapping accuracy, (2) seasonal dependency of data acquisition for mapping riparian species, and (3) cost of the data relative to their potential for improved ecosystem mapping. We evaluated those remote-sensing technologies previously determined to be worth testing and, from the results of the evaluations, developed recommendations for instrumentation and data acquisition that best meet the requirements for monitoring long-term, riparian vegetation change within the Colorado River ecosystem.

Previous Studies

There have been numerous investigations into the use of remote-sensing data for mapping vegetation that, as a whole, have considered a wide range of scales and sensor technologies. Much of this research began with the Landsat program using the spectral data in six nonthermal bands for forest and

crop inventory. These data, and other spaceborne data, are relatively inexpensive (\$0.02/km²), allowing temporal analysis to map vegetation species to an accuracy near 80% based on seasonal characteristics of the vegetation (Mickelson et al. 1998). However, the 30-m resolution provided by Landsat is too low for our mapping purposes because riparian units vary in composition and form well below the 30 m scale.

Airborne sensors can achieve much higher resolutions, generally less than 1 meter, and the cost for such data is declining (slowly) due to competition and better technology: the cost for airborne data correlates with the number of bands and spatial resolution of the data collection. Thus, remote-sensing research is moving towards the use of higher spatial and spectral resolution data in efforts to improve vegetation mapping accuracies. The following is a summary of results from recent studies describing the wavelength bands and resolutions of airborne data that have been used to map forest and riparian ecosystems and the accuracies obtained. These previous results are presented in order of increasing spatial resolution.

Trietz and Howarth (2000a) used nine spectral bands (between 0.4 μ m and 0.9 μ m) acquired from the Canadian Aeronautics and Space Institute (CASI) sensor at 6-m resolution to map coniferous forest ecosystems. Their classification accuracies were 50% on average using only spectral data, and 57-63% using both spectral and textural data. In another study, Trietz and Howarth (2000b) used a similar data set having 1 meter resolution to obtain classification accuracies of about 68% using spectral and textural data. They concluded that 5-6 meter resolution was optimal for mapping forest ecosystems in Canada; the optimal resolution varied within this narrow range among different tree species due to variations in mean canopy diameter. They also concluded that texture derived from a near-infrared band provided a superior measure of texture over that provided by visible-wavelength bands, because near-infrared energy penetrates vegetation canopy more than visible light and provides more structural information. The latter conclusion was also drawn by a previous study (Chavez 1992) that examined a wide spectrum of vegetation (coniferous and deciduous forests, agriculture, riparian, and jungle). Quackenbush et al. (2000) investigated the use of 1-m digital color-infrared (obtained from the Emerge CCD sensor) data for mapping forest stands. They achieved an average overall accuracy of 71%, with accuracies for specific vegetation units ranging from 16% to 95%. Coulter et al. (2000) used four-band (visible and near-infrared) data at 1 m resolution (obtained from the digital Airborne Data Acquisition and Registration [ADAR] 5500 sensor) and digital orthophoto quarterquads (DOQQ's) to map shrubland in southern California. They found that (1) classification accuracy of 75-80% could be obtained from the digital data, (2) classification accuracies using the DOQQ's were correspondingly lower (62-67%), and (3) post-classification field visits improved the final map accuracies by about 10%. They attributed the lower mapping accuracies obtained by the CIR photographic data to the inferior radiometric fidelity of the scanned photographic product relative to that of the digital camera. These results are supported by a more general study by Light (1996) who compared photographic and digital camera systems and determined that digital cameras provide two main advantages over photographic systems. First, digital systems can record larger dynamic ranges in radiance than film. Second, digital cameras record the reflected signals directly during data collection and retain a higher radiometric fidelity of surface radiance than do scanned photographic images. Franklin et al. (2000), using three- and five-band data in the visible and near-infrared wavelength region that were acquired at five spatial resolutions that ranged from 0.3 m to 8 m (using the digital CASI sensor), found that (1) the highest resolution images produced lower classification accuracies (by 11-25%) than the lower resolution data; (2) classification accuracies improved the most (by 15-20 %) for the highest resolution imagery when texture was added in the analysis and the amount of increase in accuracy depended on the composition of the forest stand; and (3) the classification accuracies derived from the highest resolution data (45-75%) using spectral and textural data were close to or greater than the accuracies derived from the lower resolution data. Franklin et al. (2001), using similar (1 m

resolution) data for forest mapping, obtained an overall mapping accuracy of 75%, with texture adding nearly 21% over that provided by the spectral data alone. Using even higher resolution (30 cm), three-band (green, red, and near-infrared) data Butt et al. (1998) were able to map riparian vegetation around Lake Tahoe to an accuracy of 72-74%.

In a recent study that is closely related to the present study in terms of vegetation type and geographic location, Weber and Dunno (2001) examined 2.5-m resolution data from the Airborne Terrestrial Applications Sensor (ATLAS; 14 bands between 0.45 μm and 12.2 μm) to determine how well these data could map riparian vegetation units within the Hopi Indian Reservation in northern Arizona. They found that 4 of the 14 bands (0.63-0.69 μm , 0.76-0.90 μm , 1.55-1.75 μm , and 2.08-2.35 μm) were most useful for mapping the riparian vegetation under consideration. Mapping accuracies obtained using maximum likelihood classification were about 40%. They attributed the rather low accuracies to: (1) spectral similarities of particular vegetation species (e.g., tamarisk and coyote willow); (2) ambiguities caused by an alluvium signal mixed with vegetation, even though they attempted to remove the alluvium using a vegetation index mask; and (3) the low resolution of the digital data (2.5 m) in which the compositions of units varied at smaller scales and were not detected or were confused with other units. The problems associated with spectral similarity noted by Weber and Dunno (2001) were noted as a potential problem by previous studies using vegetation spectra obtained from field spectroradiometers (e.g., Price 1994, Cochrane 2000).

Our current study examines airborne remote-sensing data that include the entire range of airborne data reviewed above to determine the capability of these data for mapping riparian vegetation along the Colorado River relative to their cost. Our databases include: (1) scanned CIR photography, digital CCD CIR imagery, and multispectral scanner data; (2) spatial resolutions from 11 cm to 100 cm; and (3) seasonal data and even data acquired under overcast sky conditions. These data are described in the following section.

Image Data and Study Sites

During the first year of the GCMRC remote sensing initiative, several remote-sensing databases were acquired that cover a range of sensor technologies and costs from scanned photographic CIR and digital CCD CIR data (both costing \$225/line km) to multispectral scanner data (costing \$620/line km). Using the Kodak DCS460CIR CCD camera (3072 x 2048; Quackenbush et al. 2000) that is operated by Emerge Corporation, airborne CIR image data were acquired in September, 1999 under clear sky conditions. These data were acquired at a stated spatial resolution of 30.5 cm, although comparison of these data with other 30 cm data suggests that the data were collected at lower resolution (closer to 60 cm) and resampled to 30.5 cm. The CCD sensor collects 3 bands (green and near-infrared, red and near-infrared, and near-infrared) and subtracts the near-infrared signal using proprietary software from the two mixed-wavelength bands to produce a three-band CIR data. The sensor records radiance as 12-bit values which are converted to 8-bit values during the post-processing phase to optimize the recorded radiance range and provide a dynamic radiance range that exceeds that of CIR film.

Color-infrared photography was acquired at three times in 2000: (1) in March under clear-sky conditions, (2) in July under clear-sky conditions, and (3) in September under uniformly overcast sky conditions. Each acquisition used Kodak Aerochrome II Infrared NP Film SO-134, whose three emulsion layers are sensitive to light within the green and blue, red and blue, and near-infrared and blue wavelength regions. The late March and early September CIR imagery were acquired at 30.5-cm and 28-cm spatial resolutions, respectively, while the early July CIR imagery were acquired at 11-cm spatial resolution,

which is the resolution that has been previously acquired by GCMRC. The three sets of CIR film were converted to digital imagery using an Intergraph PhotoScan TD Photo Digitizing System. Scanner settings (transmissivity, film density, and gamma) were set manually by visually matching image tone, contrast, and brightness on the scanned image to that observed on the film in transmitted light.

Advanced Thematic Mapper (ATM or Daedalus model 1268) data were acquired in July, 2000 between river miles (RM) 30 and 74 (river miles in the Grand Canyon are referenced to RM 0 at Lee's Ferry, Arizona). The ATM sensor collected data in 12 channels at a spatial resolution of 100 cm. The wavelength bands for the ATM channels are listed in Table 1. The signal-to-noise ratio (SNR) for each ATM channel (Table 1) was determined using the method of Gao (1993). A few of the ATM channels were not used in this study: channel 1 was too noisy (as indicated by its very low S/N ratio); channel 11 (the high-gain, thermal-infrared band) was mostly saturated due to its high gain state and the very high surface and ambient-air temperatures in the Canyon during July; and channel 12 (the low-gain, thermal-infrared band) showed extremely little variance between the various riparian vegetation units.

The Emerge CIR data and the March 2000 CIR data were provided in orthorectified form with positional accuracies of 6-8 meters and 1-2 meters, respectively, while the ATM data were provided in georectified form with positional accuracies of 2-3 meters. The remaining two data sets were provided as point-perspective, raw image data. In order to use these data with the polygon maps of the riparian vegetation that we use in this study as "ground truth" (Kearsley and Ayers 2000), the positional accuracy of the image data had to be rectified at better accuracies than that provided. A digital, orthorectified panchromatic database with 18-cm spatial resolution and a positional accuracy of 30 cm provided the control to rectify all of the image data. On average, image rectification for each selected study site required at least 35 control points and use of a first-order or second-order polynomial transformation to produce co-registration with the panchromatic image base to within one image picture element. Some study areas with more topographic relief required almost twice the average number of control points. Rectification was performed from image to map base using the State Plane coordinates for points located on the panchromatic image that could also be recognized on the multiple-band images.

The five multiple-band image data sets coincide between RM 30 and 74; this coverage was limited by the smaller coverage provided by the ATM data. Along this stretch of the Colorado River are five long-term, riparian-vegetation monitoring sites of the GCMRC. We selected all five sites for detailed analyses. These sites are shown on Figure 1 and are located at RM 43.1, 51, 55.5, 68.2, and 71.4. Delays in data delivery resulted in a lack of coverage of sites RM 51, 55.5, and 71.4 for the March film CIR and the September film CIR. However, the vegetation units in the remaining two sites (RM 43.1 and 68.2) include many of the units found at these three sites. Vegetation units within each study site are mapped annually and were most recently field mapped by Kearsley and Ayers (2000). We used their recent vegetation maps because they correspond the closest in time to our data acquisitions. Kearsley and Ayers (2000) mapped the riparian vegetation using the vegetation classification system developed by Spence et al. (1995), referred to as the SRFRC classification in this paper, which is merely the first initials of all the authors' last names. This classification system was specifically designed for the Colorado Plateau Province and largely parameterizes local vegetation series and association. The vegetation types (units) that have been mapped at the five study sites are identified in Tables 2 through 6; the genus and species corresponding to the common vegetation names are cross referenced in Table 7. Between the different study sites there is duplication of vegetation types or units, which also allows determination of the consistency with which the remote sensing data correctly or incorrectly identify a unit. The spatial distributions of the vegetation units within each study site are presented with our classification analyses of the different sites. In general, the average height and diameter of the riparian species decrease in the

order of tree, shrub, forbaceous, herbaceous, and grass. There is very little understory in tamarisk and mesquite stands, which are 3-5 meters high. Shrubs such as willows and *Baccharis* are generally about 1-2 meters high, while arrowweed averages about 1 meter in height. All three of these species form low density stands and can have grass understories. The average height of forbaceous plants are similar to shrubs, but are generally more dense.

Data Analysis

Calibration to Ground Reflectance

Recorded digital values for the nonthermal channels from the Bechtel ATM sensor were converted to ground reflectance using the empirical line method (Roberts et al. 1986, Conel et al. 1987, Farrand et al. 1994). This method correlates recorded digital band values to known band reflectance values of surface targets. In June, 2000 we conducted field spectral surveys of various geologic and vegetation materials at many locations between RM 30 and 74 using an Analytical Spectral Devices (ASD) field spectroradiometer and a Spectralon standard (presented in a later section). For image calibration we used the brightest and darkest materials within the study sites. Bright surface targets consisted of large, uniform sand bar deposits. The spectral reflectances of the sand bar surfaces at various locations along the Colorado River corridor were quite consistent. Dark objects used were areas having the lowest and most uniform digital values, such as shadowed areas in deep side canyons and deep, clear water without sun glint. The observed digital numbers of the nine ATM bands within such areas were consistent throughout this river section and were assumed to represent a reflectance of 1% because few natural surfaces have no reflectance. A third surface (a dense, closed-canopy Tamarisk grove at Nankoweap Rapids at RM 52.5) with intermediate reflectance values in some of the ATM band wavelengths was also used in order to better define the linear regression between recorded ATM band values and ground reflectance at some wavelengths. Regression of corresponding ground reflectance values and recorded digital values within each ATM wavelength band produced a gain and offset value for each Bechtel ATM wavelength band, which were then used to convert each ATM band's recorded digital values to surface reflectance.

Calibration of the Emerge digital CIR data were performed in a similar manner to that of the Bechtel MS data. The CIR film was not digitized using the same scanner settings, which would have maintained some consistency in image values along the river corridor and would have allowed extrapolation of ground-truth spectral data between study sites. Rather, scanner settings were chosen independently for each flight line of film to optimize information content. In addition, atmospheric scattering within the three different wavelength regions recorded by the Kodak film could not be reliably estimated because the Kodak SO-134 film emulsions for the green, red, and near-infrared wavelengths are also sensitive to the blue wavelength. Thus, shadow areas without vegetation could have near-infrared digital values similar to areas of dark or shaded vegetation. Calibration of the film-derivative image data was therefore accomplished by correlating ground reflectance observed in the Bechtel wavelength bands to recorded digital values in the film-derivative image data using bright and dark surface targets and uniform, closed-canopy vegetation as reference targets within each study area. This required convolving the Bechtel ATM wavelength bands to corresponding CIR film wavelengths.

In order to restrict our classification analyses to only vegetation, we created NDVI (Normalized Difference Vegetation Index) images from each color database for each study area. We used the smallest occurrence of vegetation observable in each color image as targets for determining the lowest NDVI value that represented mostly vegetation. Where possible, the same target area was used for determining this

NDVI value in all five image databases. Within a particular study site the derived NDVI values for the five different color databases were very similar, but did differ somewhat between study areas, possibly due to differences in the target vegetation. These derived vegetation masks were then used to delete picture elements in the image databases and in the ground-truth vegetation maps that were not vegetated. It has been shown that isolation of the specific material of interest can improve classification results (Hutchinson, 1982).

Texture Analysis of Remote-Sensing Data for Vegetation Discrimination.

Different species of vegetation can exhibit textural variations in image data due to differences in their branch (canopy) structure and average plant spacing (density). Differences in image texture between species have been used to supplement spectral data in the classification of vegetation (e.g., Lacaze et al. 1984, Franklin et al. 2000, 2001). For example, changes in variance as a function of distance from an object (referred to as a semivariogram) are useful in discrimination between various vegetation species (Woodcock et al. 1988a, b). Generally, the addition of texture in spectral classification of vegetation increases the classification accuracy by 10-15% relative to the accuracy obtained using just spectral band data (Franklin and McDermid 1993, Franklin et al. 2000, 2001). There have been instances, however, where the addition of texture had little effect on the accuracy of the results (Franklin and McDermid 1993, Franklin et al. 2000, 2001). In general, forest-mapping classification accuracies in the range of 65-80% have been obtained with spectral and textural data using co-occurrence filters. Co-occurrence filters examine the similarity of values between two rectangular areas separated by a particular distance. A variety of mathematical treatments of the data within both co-occurrence rectangles have been devised (Haralick et al. 1973); a few of these algorithms have proven to be more useful than others (e.g., entropy, contrast, and inverse difference moment). A disadvantage of co-occurrence filters is that they require at least one to two orders of magnitude more processing time than the more common occurrence filters (e.g., variance, mean, range, skewness). We performed some preliminary classification tests using co-occurrence and occurrence filters for variance and entropy on some study areas and found that co-occurrence filters did not markedly increase the classification accuracies relative to the results obtained using corresponding occurrence texture filters. Thus, our study concentrated on occurrence texture filters.

Tests of various occurrence texture filters show that variance was one of the most useful measures for discriminating vegetation units within the study areas. Entropy provided only slightly better discrimination (1-2% absolute accuracy increase over variance), but the entropy algorithm requires significantly more processing time than variance. Because bare ground was removed from the image data and set to zero, texture filters will produce anomalously high values at the edges of the vegetated (non-zero) picture elements. In order to eliminate this edge effect with the texture filters, we redesigned the variance filter to consider only non-zero data in its calculation of variance. A series of variance filters using different cell dimensions were performed on the near-infrared band of all five color image databases. Previous research has shown that near-infrared bands provide the most vegetation texture information (Chavez 1992, Trietz and Howarth 2000b). The filter dimensions tested ranged from 39 (picture elements) to 99 for the 11 cm data, 19 to 51 for the 30 cm data, and 3 to 31 for the 100 cm data, in increments of two picture elements. Our preliminary assessment of vegetation-unit texture at small dimensions (less than 3-5 meters) suggested that texture at such very small scales picks up too much intraspecies variations. The change in unit variance as a function of filter dimension is shown for two examples in Figure 2. The change in variance with filter dimension for vegetation unit 5 in Figure 2b is similar to that seen in variograms. Many of the databases for each study site produced unit variance distributions that cross, which helped define the filter dimension to provide optimum unit discrimination. There were instances, however, where unit variance distributions derived from a particular image

database for a study site were a set of parallel lines, which were not useful in defining an optimum filter dimension. The filter dimension that provided the best separation between the units in the former cases could be determined visually, but we sought numerical confirmation of the exact filter dimension to make this analysis less subjective.

For each study area, we statistically examined the variance results for each color image database to determine the filter dimension that best discriminated between the vegetation units. The best filter dimension will produce average unit variance values that have (1) a large range and (2) a uniform, maximum spacing between unit variance within that range. The maximum spacing in variance for a given range in variance is: $space_{max} = range / (n-1)$, where n is the number of vegetation units. A measure of how close the set of unit variance values approach this maximum spacing for a given filter dimension was calculated in four steps: (1) determine the percentage of each unit's variance within the range of variance found at the site, (2) numerically order these percentage values and subtract adjacent values, which results in n-1 values, (3) subtract $space_{max}$ (derived above) from each value, and (4) sum the absolute values from (3). This sum ($space_{diff}$) yields a numerical measure of the degree to which the set of unit variances approaches maximum spacing for a particular filter dimension. The smaller the value of $space_{diff}$, the closer the set of unit variances approaches maximum separation within the range of data. Uniformity of separation of a set of unit variance values ($space_{dev}$) was determined by calculating the standard deviation of the set of absolute differences obtained in step (3). The overall quantitative measure of the degree of discrimination provided by a particular filter dimension was determined by the relation: $discrim = (range\ in\ variance) / (space_{diff} \cdot space_{dev})$. The filter dimension that results in the largest *discrim* value will be the most useful filter for unit discrimination for that particular study area. The optimum filter dimensions resulting from our analyses of all image databases for all five study sites are plotted as a function of image resolution in Figure 3. These values were subjected to least squares analyses to determine the equation that best represented the graphical relation. A power law provided the best solution ($R^2 = 0.933$); the least-squares equation is provided in Figure 3. This equation was used to set the dimension for texture analysis of the near-infrared image from each multiple-band image database, which was then used with the spectral band data in our classification analyses.

To verify our results for selection of an optimum texture filter dimension and to determine if a combination of variance filters may produce better classification results than a single texture filter, we produced two additional variance images using filter dimensions that were one-third and two-thirds of the dimension of our derived optimum filter dimension. These additional filters were applied to the 11-cm CIR image data, the 30.5-cm Emerge data, and the 100-cm ATM data for study sites RM 51, 55.5, and 71.4. These sites were selected because our preliminary analyses indicated these sites present cases where texture greatly improved classification accuracy (RM 55.5 and 71.4) and where texture had little effect (RM 51). We applied a maximum likelihood classifier to the spectral band data using each of the two intermediate texture images individually, then using all three texture images with the spectral band data. The results showed that only the classification employing all three texture images and the spectral band data exceeded the classification accuracy produced by using only the optimum texture image with the spectral band data. However, the increase in accuracy provided by the two additional texture databases was less than one absolute percent. Thus, the single optimum texture image was used in our classification analyses of the study sites.

Classification of Remote Sensing Data

Various supervised classifiers (Mahalanobis distance, maximum likelihood, minimum distance, spectral angle mapper, parallelepiped) were tested on the different databases to determine which classifier

provided the highest accuracy. We found maximum likelihood consistently produced the highest accuracies and this method was used in all of the subsequent analyses. Supervised classification requires training areas to obtain statistics from the remote-sensing databases for the materials to be mapped. For each study site, training areas were established for each vegetation unit using the map polygons established by Kearsley and Ayers (2000) and thus the same training areas were used for all image data for a particular study area. Our initial classification analysis used only the spectral bands from each image database. Our second classification analysis used both the spectral bands and the near-infrared texture image from each image database. The overall accuracies obtained from both of these analyses are shown in Table 8.

The following observations can be made relative to vegetation classification using only spectral band information.

1. The ATM nine-band data produce the highest overall classification accuracies of all image databases used in this analysis, with the exception of study site RM 43.1 where the accuracy from the 11-cm image data is greater than that obtained from the ATM data.
2. Overall classification accuracy generally decreases with higher spatial resolution data in the 10-100 cm range, except at study site RM 43.1. The greater spatial detail provided by the highest resolution data may exceed that used to map the vegetation units in the field. The inverse relation between classification accuracy and spatial resolution has been observed in other studies (e.g., Franklin et al. 2000). The lower resolution image data average more of the surface during radiance collection, thus reducing interunit spatial variation seen by higher resolution data and consequently reducing the probability for mis-classification of vegetation units.
3. Not considering the September CIR film data that were acquired under overcast sky conditions, the accuracies obtained from the 11-cm and 30-cm data acquired under clear-sky conditions in the Spring, Summer, and Fall seasons are not appreciably different. Thus, there does not appear to be a seasonal bias for mapping the riparian vegetation.
4. The September, 2000 28-cm CIR data for the five study sites produced the lowest classification accuracies of all five of the image databases that were investigated. Two factors might account for this. First, the vegetation may have had lower chlorophyll contents at that time due to senescence. However, the higher accuracies provided by the March 2000 CIR film and September 1999 Emerge data, both having comparable spatial resolutions to that of the September 2000 data, negate this possibility. Second, the September 2000 CIR data were acquired during totally overcast sky conditions and, therefore, the reduced solar flux and resultant reduced surface reflectance may produce less spectral contrast between the different vegetation species.
5. Some of the classification accuracies are close to accuracies recently obtained (40%) in a classification study of similar riparian vegetation in Arizona (Weber and Dunno 2001), which used 2.5-m four-band (green, red, near-infrared, and two short-wave infrared bands) multispectral data. However, many of the accuracies obtained from our image data are higher than 40%, which is attributed to the higher spatial resolution (≤ 100 cm) provided by our data. Therefore, there is a point at which reduced spatial resolution produces lower classification accuracy, which depends on the scale of the surface units.
6. Unlike some previous studies (e.g., Coulter et al. 2000), we do not observe a large difference

in the accuracies produced by the film-derived CIR versus the digital Emerge CIR at comparable resolutions. This is probably due to our radiometric calibration of these data prior to classification. Calibration is time consuming and, in terms of total expense, it would be preferable to use image data that provided radiometric fidelity without post processing, especially for high-resolution image data for large areas.

With respect to the classification accuracies obtained using both spectral bands and texture, we make the following observations from Table 8.

1. The addition of texture increases classification accuracy in almost every case. The increase is greatest for the highest resolution data (11 cm) and least for the lowest resolution data. The increase in accuracy using the highest resolution data (11 cm) ranges from 5% to 30%, with three of five study areas showing increases of 20-30%. Both results have been found in previous forest classification studies (e.g., Franklin et al. 2000, 2001).
2. The accuracies obtained using the highest resolution image data with texture are greater than that obtained from all other lower resolution data and even exceed the overall accuracies obtained from the 100-cm ATM data for two of the five study sites where overall accuracies obtained using spectral band data alone were closest between the 11-cm and 100-cm data.
3. Classification accuracies obtained from our riparian vegetation study sites are comparable to those obtained from classification analyses of forested regions (Franklin and McDermid 1993, Franklin et al. 2000, 2001).

The overall classification accuracies reported above are derived by dividing total correctly classified picture elements by the total number of picture elements in the image area. Thus, the overall classification accuracy is determined mostly by the highly populated units and may not reflect a large mis-classification of individual units. This is shown in Table 8, which lists the classification accuracies obtained for the individual vegetation units using both spectral band and texture data. It was noted above that the overall classification accuracies obtained using the September 2000 data (overcast sky conditions) were uniformly lower than the results from all other databases. Table 8 shows that the results obtained for many vegetation units using the September 2000 data are as good as, and in some cases better than, those obtained from the other CIR film data and from the digital CIR and ATM sensors. This is most marked for study site RM 68.2 (Table 8). This suggests that data acquisition during overcast sky conditions would not be detrimental for mapping certain vegetation units, but such data would not provide the best overall classification map.

The unit accuracies in Table 8 also show that the classification results provided by the 100-cm ATM data are not only generally higher but are also uniformly higher than the unit accuracies provided by the film and digital CIR data. The 11-cm CIR film data produce more occurrences of large discrepancies in unit accuracy relative to the accuracies obtained from the ATM data. These occur for vegetation units 1 and 5 at RM 43.1, unit 2 at RM 51, unit 5 at RM 55.5, and unit 5 at RM 68.2 (Table 8). These vegetation units are the less densely populated and generally occur as scattered patches of vegetation on alluvium. Thus, the small statistical base provided by these patchy units may not provide a spectral signature that is distinct from other units. The March and September CIR film data do not show most of these large discrepancies in unit accuracy, except for vegetation unit 5 at RM 43.1. These two CIR data were acquired at much lower sun elevation angles than the July CIR data and the film scanning process may have saturated these scattered vegetation patches so that their true radiance characteristics

were lost and made similar to other highly reflective units. Overall, the digital Emerge CIR data produce much better results for these small, scattered units, which suggests that radiometric fidelity (capability of recording over a large radiometric range) is an important factor for attaining high accuracies for all vegetation units.

Examination of the classification maps for study site RM 43.1 (Figures 4-10), specifically those obtained from the 11-cm film CIR data and the ATM data, shows that both data sets mapped much of vegetation unit 1 as unit 2. Both vegetation units contain tamarisk, but unit 1 has tamarisk as a subordinate member (Table 2). Their confusion, and the resulting low accuracies for unit 1 are understandable. The 11-cm film CIR data classified most of vegetation unit 5 (coyote willow, dicoria, and russian thistle) as unit 4 (cattail and phragmites). The sparse nature of both of these units and saturation during film scanning due to the dominance of alluvium in these units may not have produced distinct signatures for the two units. The ATM data mapped much of unit 5 as unit 3 (coyote willow, equisetum, and Baccharis). The spectral signatures of these two willow units may not be sufficiently different to allow discrimination by the classifier. The classifier took the signature of the more-populated unit 5 as truth, but this type of mis-classification can be handled by post-processing analysis, whereas the mis-classification of unit 5 as a wetland (marsh) unit by the 11-cm film CIR data would require more field verification and adjustments.

Within study site RM 51 (Figures 11-15), the 11-cm film CIR data could not distinguish between the units dominated by acacia shrubs (vegetation unit 2) and tamarisk (vegetation unit 3) and mapped much of unit 2 as tamarisk. This is a problem in the classification map produced using the Emerge data as well. Both the 11-cm film CIR and the 100-cm ATM data map much of the shoreline occurrences of tamarisk (vegetation unit 3) and coyote willow and Baccharis (vegetation unit 4) as vegetation unit 5 (cattail and rush). Unit 5 occurs only as sparse, scattered exposures, as do the shoreline occurrences of units 3 and 4, so that the signature for unit 5 must have been given more weight in the classifier. The Emerge 30.5-cm data mapped unit 4 better than these other data, suggesting that calibrated data with at least 30 cm resolution may be necessary to distinguish such sparse, scattered occurrences of vegetation.

Within study site RM 55.5 (Figures 16-20), the 11-cm film CIR data classified much of vegetation unit 5 (sedge and rush) as unit 1 (phragmites and bent grass). Both the 11-cm film CIR and the 30.5-cm Emerge CIR data over-represent the occurrence of unit 4 (mesquite and acacia). On the other hand, the ATM data map large areas of tamarisk (unit 2) as willow and Baccharis (unit 3), however, vegetation unit 2 has subordinate Baccharis and the ATM may be mapping local concentrations of Baccharis. Weber and Dunno (2001) reported a problem in distinguishing tamarisk from willow, but we did not have this problem in our other study sites that have both types of vegetation.

Within study site 68.2 (Figures 21-27), vegetation unit 5 (cattail and rush) is under-represented in the classification maps produced by all five data sets. The largest single exposure of unit 5 is mapped mostly as unit 1 (coyote willow, Baccharis, and equisetum). The cattail and rush unit occurs where there is a high percentage of alluvium and removal of the alluvium using the NDVI may not have been complete. The March 30.5-cm film CIR data produced the only map that depicts this exposure, in addition to other shoreline exposures. The lower contrast provided by that data, which were acquired under overcast sky conditions, may have produced much less overexposure during the film scanning process. All image data sets produce confusion between vegetation units 1 and 2; both vegetation units have willow as a dominant member and their separation by their subordinate species (Table 5) may not be possible.

Within study site RM 71.4 (Figures 28-32), both the 11-cm film CIR and 30.5-cm Emerge CIR over-represent vegetation unit 1 (phragmites and rush), mostly where unit 3 (arrowweed and camel thorn) occurs, but the 11-cm film CIR data do this much less so than the Emerge data. Overall, there are very little differences between the maps produced by the 11-cm film CIR data and the ATM data at this site.

In addition to radiometric fidelity, the consistently higher accuracies provided by the Bechtel ATM data can also be attributed to the larger amount of spectral information provided by the nine ATM bands relative to that of three CIR bands. However, sensors that provide the short-wave infrared bands (e.g., the 1.69 μm and 2.25 μm bands within the ATM database) are more expensive for data acquisition than visible/near-infrared-wavelength sensors because the short-wave infrared bands require additional detectors. Thus, we determined the relative importance of the nine ATM bands in mapping the riparian vegetation units by conducting classification analyses of the ATM data. The first series examined the effect of omitting a single ATM band. The band that produced the least effect on accuracy was selected for omission in subsequent analyses, as long as the decrease in accuracy from the original nine-band results was less than 10%. Each subsequent series of analyses excluded the previously selected bands and each one of the remaining ATM bands individually. All of these analyses included texture data. The analyses ceased for a particular study area when all of the remaining bands to be omitted produced a decrease from the original accuracy by greater than 10%. This process showed that the least useful ATM bands include bands 2, 5, 8, and 9. This left ATM bands 3, 4, 6, 7, and 10 (see Table 1 for wavelengths). The unit classification accuracies for each study site using this reduced band set are very close to that obtained using all nine ATM bands (Table 9).

To determine the importance of including the remaining short-wave band (ATM band 10) in the classification, we performed classification analysis for each study site using only ATM bands 3, 4, 6, and 7. The results are compared with those using the reduced five-band and the full nine-band ATM data in Table 9. Examination of the results from the reduced four-band ATM data indicates that there are three units with accuracies that are about 10% or more lower than the unit accuracies obtained from the full nine-band ATM database (Table 9) and that overall accuracies for the study sites are only 3-7% lower than those obtained from the nine-band ATM data. Comparison of the classification maps produced by the reduced four-band ATM data set with those produced by the full nine-band ATM data set show that the two data sets produce very similar spatial results (e.g., Figures 33-37).

Of all the bands within the reduced four-band ATM database, the omission of band 4 has the least effect of total unit accuracies; classification results using only ATM bands 3, 4, and 6 are also shown in Table 9 for comparison. There are seven units in all of the five study areas that have accuracies of 10% or more lower than those obtained from the full ATM database, but only one corresponds to the three low unit accuracies observed in the four-band results. In fact, the accuracies for vegetation units 4 and 5 in study site RM51 actually increased by excluding ATM band 4 (Table 9). This reduced three-band database consists of wavelength bands that are very similar to conventional CIR sensors. For comparison, we also show our previous classification results obtained using the 11-cm film CIR band and texture data (Table 9). There are only two cases (vegetation unit 2 at site RM 51 and vegetation unit 1 at site RM 71.4) where lower accuracies coincide in the 11-cm film CIR film results and in the reduced three-band ATM results. Thus, a combination of well-calibrated data (such as produced by the ATM sensor) at a higher resolution (for better texture data) may approach or even match the accuracies provided by the nine-band ATM data, whose results are within the range of accuracies obtained in recent forest classifications. Texture derived from 30-cm data appears to only add about 5% accuracy (Table 8). The use of data with resolutions better than 30 cm seems warranted on a purely textural basis, however, 11-cm digital data collection for the entire 476-km long river corridor will be extremely expensive, commencing with data

acquisition and magnifying throughout the data storage and data processing phases. In addition, higher classification accuracies appear to be obtained at resolutions lower than 11 cm when only spectral data obtained from calibrated, digital sensors are considered (such as the Emerge CDD and ATM scanner; Table 8).

In order to determine if image data with a resolution between 11 cm and 30 cm could provide valuable textural information for increased image classification, we digitally reduced the spatial resolution of the 11-cm CIR film data using a Gaussian filter to produce CIR data with a 20-cm resolution for each study site. Using these data for each site, texture was derived from the near-infrared band and used with the reduced-resolution CIR band information in maximum likelihood classification. The results from these analyses indicate that classification accuracies obtained at the 11-cm scale were maintained at the 20-cm scale and that improvements in classification accuracy due to texture were comparable to those obtained using 11-cm image data. The fact that the accuracies did not increase at lower spatial resolution using the same data also suggests that decreased resolution alone does not improve classification results and that radiometric performance of a sensor is a major factor in achieving high mapping accuracies from remote-sensing data.

Higher resolution image data present more area of shaded vegetation within an image and thus a higher probability for mis-classification of shaded picture elements using band reflectance data. In an attempt to overcome this potential problem, we examined the use of band ratios in all of the CIR band data because band ratios may normalize the effects of canopy topography to a first order. Theoretically, band ratios should produce better classification accuracies if canopy shading is a primary issue and if the image signal-to-noise ratios are relatively high, otherwise the noise within the data can produce poorer results. We found, for all five study areas, that the majority of classification accuracies for the vegetation units obtained from band ratios and texture were lower than those obtained using band reflectance and texture data, except for the ATM data. This suggests that albedos of the vegetation species are more important for accurate classification than the relative reflectance differences between bands, agreeing with observations made using field spectral data (Cochrane 2000, Weber and Dunno 2001). These results also further reinforce the importance of obtaining image data with sensors that can record a wide dynamic range of radiance.

Field Spectroradiometric Data Analysis

During June and September of 2000 we acquired spectroradiometric measurements of many vegetation species between RM -15 and 60 along the Colorado River. The field measurements were obtained using an Analytical Spectral Devices (ASD) spectroradiometer that records spectral radiance between 0.4 μm and 2.5 μm in intervals of 0.001 μm . Data were collected in two ways. First, a spectrum was acquired of the in-situ plant. Second, leaves from the plant were extracted and placed on a flat, black plate, covered by a clear glass plate that was used to compress the leaves to a flat surface, and a spectrum was acquired of the compressed plant. This method removes the possible radiance from the understory ground that might contribute to the in-situ measurements. After each in-situ and black-plate measurement, a spectrum of a Spectralon white standard whose geometric orientation to the Sun matched that of the sample was acquired. The Spectralon standard spectrum for a sample was used to normalize the sample measurement and to produce a reflectance spectrum of the sample.

The resulting collection of vegetation spectra were examined to determine intraspecies variation and to form average reflectance spectra for a species sample collection that had similar spectral characteristics. Samples of a plant species that were anomalous were maintained as separate reflectance

spectra for further analysis. Our sample collection consisted of 21 different plant species and a total of 45 reflectance spectra that included spectral variations of particular species. These 45 sample spectra were subjected to a statistical analysis to determine the combination of wavelength bands that provided the best discrimination among the sample collection. The analyses were performed using a three-band and a four-band approach. The statistical measure of discrimination used in our analyses was the determinant of the correlation matrix formed by a particular three- or four-band combination (Crippen 1989). The analysis algorithm iterated through all possible wavelength bands that can be formed between 0.5 μm and 2.4 μm , with wavelength bandwidths varying between 0.02 μm and 0.10 μm . These analyses did not consider the blue wavelength (0.4-0.5 μm) or the short-wave-infrared wavelength (2.4-2.5 μm) bands because of inherent high noise levels. Two sets of analyses were performed for both the three- and four-band cases; one set of analyses considered only the 0.5-1.0 μm region and the other set of analyses considered the entire 0.5-2.4 μm region. These two separate analyses were used to evaluate the relative merits of using more sophisticated sensor data (i.e., more expensive data) that could acquire spectral data within the short-wave infrared region between 1.0 μm and 2.4 μm . The following observations and conclusions summarize the results from these analyses of the plant spectral data.

1. Three-band and four-band spectral analyses for the 0.5-1.0 μm region produced consistent band centers regardless of bandwidth. The three-band analysis indicated that maximum discrimination of the riparian plant species are achieved using bands centered within the following ranges: 0.53-0.54 μm , 0.66-0.67 μm , and 0.79-0.815 μm (wavelength centers shown in Figure 38). The four-band analyses indicated an additional band center at 0.70 μm (Figure 38), but this fourth wavelength band did not produce a higher determinant value (better theoretical discrimination) than the three bands listed above.
2. Three-band and four-band spectral analyses for the 0.5-2.4 μm region also produced consistent band centers regardless of bandwidth. The three-band analysis indicated that maximum discrimination of the riparian plant species are achieved using bands centered within the following ranges: 0.52-0.54 μm , 0.78-0.80 μm , and 2.02-2.07 μm (wavelength centers shown in Figure 39). The first two of these band-center ranges nearly coincide with two of the band centers indicated by the analyses within the 0.5-1.0 μm region. The four-band analyses within the 0.5-2.4 μm region indicated an additional band center in the range of 1.64-1.67 μm (Figure 39).
3. The optimum four-band determinant value obtained from the 0.5-2.4 μm wavelength region was much higher than the optimum four-band determinant obtained from the 0.5-1.0 μm wavelength region. This suggests that the addition of a short-wave infrared wavelength band would produce better vegetation discrimination (and possibly higher accuracy) than the addition of another visible or near-infrared wavelength band.
4. Three- and four-band determinant analyses indicated optimal band centers that are very close to the Bechtel ATM band centers that proved most useful for three- and four-band classification of riparian vegetation in our study areas, with the most useful set of ATM bands for classification of riparian vegetation centered at 0.55 μm , 0.69 μm , 0.79 μm , and 2.25 μm .
5. The results from the determinant analyses seem to prefer very narrow bandwidths (0.02 μm), but in practical applications for imaging at high spatial resolution (required for GCMRC) it may be necessary to use broader wavelength bands to increase signal-to-noise ratios due to the short dwell (integration) time of the sensor over a particular picture element. Broader wavelength

bands (0.05-0.06 μm in width) do not significantly lower the determinant ranking of a particular band combination.

6. In terms of ambiguities in spectral discrimination, the three-band spectral approach restricted to the 0.5-1.0 μm region may not be able to distinguish between sedge, sand sage, and rush and between grass or sedge and blue tamarisk. The first ambiguity is not an important issue, and the second ambiguity can be resolved using texture because the texture of tamarisk is very different from that of grass and sedge. The addition of the fourth optimal band within this spectral region presents these same ambiguities. Thus, there is no justification for using a fourth band within the 0.5-1.0 μm region. Using an optimal band above 1.0 μm presents fewer ambiguities, but inclusion of a short-wave infrared band may also increase the cost for data collection.

Cost-benefit analysis

Field surveys during 1999 covered 11 study sites. The average length of the study sites was about 0.45 km resulting in a total survey length of about 5 km. The cost for the surveys for the 11 sites was about \$79,000, including post-field analysis, which equates to a cost of about \$16,000/site-km. Assuming that classification of appropriate remote-sensing data can conservatively provide mapping accuracies near 60% (although our mapping accuracies may be understated as discussed below), subsequent field surveys would have to spot check the results and may have to apply conventional survey methods to parts of the study sites. The cost of the remote-sensing data acquisition and analysis may be about \$700/site-km, resulting in a total (field and remote-sensing) cost for an annual riparian mapping campaign of about \$8,700/site-km, assuming field work is about 50% more efficient using preliminary classification results from remotely sensed data. The lower cost for a combined remote-sensing and field approach would therefore allow almost twice as much monitoring per year for the same current expenditure. The cost for the data acquisition (approximated at \$350/site-km) that is factored into this analysis is probably high because other monitoring programs make use of the remote-sensing data.

The cost-benefit of using remotely sensed data for mapping riparian vegetation may be understated in this study because our remote-sensing results are being compared with vegetation maps compiled by Kearsley and Ayers (1999). Although mapping vegetation collections generally produces higher accuracies than mapping individual species, there are many "mis-classifications" in our remote-sensing results due to the ability of the remote-sensing data to identify individual stands of a species within a collection of vegetation as defined by Kearsley and Ayers (1999). Visual mapping techniques are highly contextual, whereas computer classifications do not consider context (except texture). At some point in the classification procedure using remotely sensed image data, it might be better to refine the computer classification maps using visual interpretation as is used by the field botanists. This post-classification analysis should significantly increase the mapping accuracy (in terms of correspondence to current vegetation collections) and further reduce the field survey costs. Before that is attempted, the accuracy of single-species identification by the classifier should be verified in the field.

Conclusions

This study examined various airborne remote-sensing data that were collected during different seasons within a one-year time frame, at different spatial resolutions (11 cm to 100 cm), and using various technologies (CIR film, CIR CCDs, and multispectral data) to determine the relative merits of each data set for mapping riparian vegetation within the Grand Canyon. The results of this study indicate the following:

1. Intrinsic brightness (reflectance) is an important factor in discrimination of riparian vegetation. Thus, digital cameras that can record a large range of radiance produce better classification accuracies than scanned film data because the scanning process typically cannot represent the true radiance range presented by the vegetation and bright sand surfaces found along the Colorado River. In addition, digital sensors that maintain high radiometric fidelity with respect to surface radiance will produce higher classification accuracies than sensors that are not well calibrated.
2. Although the CIR film data acquired with overcast sky conditions produced classification accuracies for individual vegetation units comparable to that obtained using film and digital CIR data acquired under clear sky conditions, overall classification accuracy resulting from the overcast image data set was lower. Although vegetation shading under overcast conditions is minimized or non-existent, the lower vegetation reflectance seems to be a more significant factor in classification accuracy than the absence of shaded vegetation. Data acquired around the winter solstice may also suffer from shadows cast by the steep canyon walls. Therefore, clear-sky data acquisition near the summer solstice (within 3-4 weeks of the solstice) should be a collection priority. In terms of time of day, a 3-4 hour window centered at local noon minimizes shadows cast by the canyon walls, which are very steep in several reaches.
3. The inclusion of texture with band reflectance improves classification accuracies by 20-30% for the high-resolution data and much less markedly for lower resolution data. The classification results using texture and band reflectance of the 11-cm film CIR data exceeds those from 30-cm film and digital CIR data and approaches those obtained using the full nine-band ATM data set. Reduction of the 11-cm data to 20 cm spatial resolution appears to maintain the proportional benefits of texture with respect to classification accuracy, thus 20-cm spatial resolution appears to be a useful spatial resolution for data acquisition.
4. Study-site classification accuracies of 52-74% produced using a four-band subset of the nine-band ATM data (0.52-0.59 μm , 0.59-0.62 μm , 0.67-0.72 μm , 0.73-0.85 μm) are comparable to those produced using the full set of nine ATM bands. A further reduced set of band data that excluded the 0.59-0.62 μm band produced accuracies for several vegetation units that are 10% less than that obtained from the analysis of the full nine-band ATM data set. These results suggest that a set of three to four visible/near-infrared bands can produce classification accuracies comparable to a multispectral sensor, but use of four bands produces more reliable results. Multispectral scanner systems that provide short-wave bands cost between \$620/line km and \$1,000/line km for data acquisition, whereas digital CCD sensor that provide three to four wavelength bands in the visible/near-infrared region cost about half as much. Thus, accepting only slightly lower classification accuracies using a four-band CCD sensor will lower an operating budget by 50% over that using more sophisticated technology that offers only slightly better results. The use of radiometrically calibrated, digital remote-sensing data in initial mapping efforts that may provide 60% accuracy, followed by field verification and possible conventional field surveys of the remaining 40% of a study area, show that annual monitoring costs for riparian habitats can be reduced by a factor of two over the current in-situ monitoring approach.

Recommendations for Future Remote-Sensing Monitoring of Riparian Vegetation

1. Wavelength Bands - Three bands, centered within the wavelength regions of 0.53-0.54 μm ,

0.66-0.67 μm , and 0.79-0.815 μm , should be used for classifying the riparian vegetation. Where four-band sensors are available, a preference for the fourth wavelength band center should be either at 0.70 μm or near the 2.02-2.07 μm wavelength region, where different riparian species also display distinctly different amounts of reflectance.

2. Sensor - A digital sensor should be used that provides radiometrically calibrated image data. Calibrated image data will significantly increase classification accuracies and decrease costs associated with the classification process. A two-dimensional CCD array sensor is preferred over a linear CCD array sensor because the former produces less geometric distortion.

3. Spatial Resolution - Image data should be acquired at a resolution near 20 cm per pixel to retain the textural information for typical riparian vegetation.

4. Time of Acquisition - Data should be acquired near summer solstice in order to minimize shading within vegetation, to minimize shadows cast over vegetation by canyon walls, and to provide a large sun-elevation window for daily image acquisition.

5. Positional Instrumentation - Data should be acquired using an accurate Global Positioning System (GPS) and Inertial Measurement Unit (IMU) that can provide at least sub-meter positional accuracy and preferably near 30 cm positional accuracy.

6. Rectification - All image data should be orthorectified. It might be advantageous for only individual frames to be rectified so that changes in sun elevation can be considered by the analysts. Commercial firms cannot generally produce digital image mosaics that are radiometrically controlled over large distances.

References Cited

- Butt, A. Z., M. B., Ayers, S. Swanson, S., and P. T. Tueller. 1998. Relationship of stream channel morphology and remotely sensed riparian vegetation classification. Pages 409-416 in American Water Resources Association Technical Publication Series TPS-98-1.
- Chavez, P. S. 1992. Comparison of spatial variability in visible and near-infrared spectral images. *Photogrammetric Engineering and Remote Sensing* 58:957-964.
- Cochrane, M. A. 2000. Using vegetation reflectance variability for species level classification of hyperspectral data. *International Journal of Remote Sensing* 21:2075-2087.
- Conel, J. E., R. O. Green, G. Vane, C. J. Bruegge, and R. E. Alley. 1987. AIS-2 radiometry and a comparison of methods for the recovery of ground reflectance. Pages 18-47 in G. Vane, editor, *Proceedings -- 3rd Airborne Imaging Spectrometer Data Analysis Workshop*, Jet Propulsion Laboratory Publication 87-30. Jet Propulsion Laboratory, Pasadena, CA.
- Coulter, L., D. Stow, A. Hope, J. O'Leary, D. Turner, P. Longmire, S. Peterson, and J. Kaiser. 2000. Comparison of high spatial resolution imagery for efficient generation of GIS vegetation layers. *Photogrammetric Engineering and Remote Sensing* 66:1329-1335.
- Crippen, R. E.. 1989. Selection of Landsat TM band and band-ratio combinations to maximize lithologic

- information in color composite displays. Pages 917-921 in Proceedings -- 7th Thematic Conference on Remote Sensing for Exploration Geology. Environmental Research Institute of Michigan, Ann Arbor, MI.
- Farrand, W. H., R. B. Singer, and E. Merenyi. 1994. Retrieval of apparent surface reflectance from AVIRIS data: A comparison of empirical line, radiative transfer, and spectral mixture methods. *Remote Sensing of Environment* 47:311-321.
- Franklin, S. E., R. J. Hall, M. Moskal, A. J. Maudie, and M. B. Lavigne. 2000. Incorporating texture into classification of forest species composition from airborne multispectral images. *International Journal of Remote Sensing* 21:61-79.
- Franklin, S. E., A. J. Maudie, and M. B. Lavigne. 2001. Using spatial co-occurrence texture to increase forest structure and species composition classification accuracy. *Photogrammetric Engineering and Remote Sensing* 67:849-855.
- Franklin, S. E., and G. J. McDermid. 1993. Empirical relations between SPOT HRV and CASI spectral response and lodgepole pine (*Pinus contorta*) forest stand parameters. *International Journal of Remote Sensing* 14:2331-2348.
- Gao, B-C. 1993. An operational method for estimating signal to noise ratios from data acquired with imaging spectrometers. *Remote Sensing of Environment* 43:23-33.
- Haralick, R. M., K. Shanmugan, and I. Dinstein. 1973. Textural features for image classification. *IEEE Transactions on Systems, Man, and Cybernetics* 3:610-621.
- Hutchinson, C. F. 1982. Techniques for combining Landsat and ancillary data for digital classification improvement. *Photogrammetric Engineering and Remote Sensing* 48:123-130.
- Kearsley, M. J. C., and T. J. Ayers. 2000. Riparian vegetation monitoring in the Colorado River Corridor 1998 to 1999. Report to Grand Canyon Monitoring and Research Center, Biologic Program. U.S. Geological Survey, Flagstaff, AZ. 47 pp.
- Lacaze, B., S. Rambal, and T. Winkel. 1994. Identifying spatial patterns of Mediterranean landscapes from geospatial analysis of remotely-sensed data. *International Journal of Remote Sensing* 15:2437-2450.
- Light, D. L. 1996. Film cameras or digital cameras? The challenge ahead for aerial imagery. *Photogrammetric Engineering and Remote Sensing* 62:285-291.
- Mickelson, J. G., D. L. Civco, and J. A. Silander. 1998. Delineating forest canopy species in the northeastern United States using multi-temporal TM imagery. *Photogrammetric Engineering and Remote Sensing* 64:891-904.
- Phillips, B. G., A. M. Phillips, and M. A. Schmidt-Bernzott. 1987. Annotated checklist of vascular plants of Grand Canyon National Park. Grand Canyon Natural History Association Monograph Number 7. 79pp.

- Price, J. C. 1994. How unique are spectral signatures? *Remote Sensing of Environment* 49:181-186.
- Quackenbush, L. J., P. F. Hopkins, and G. J. Kinn. 2000. Developing forestry products from high resolution digital aerial imagery. *Photogrammetric Engineering and Remote Sensing* 66:1337-1346.
- Roberts, D. A., Y. Yamagushi, and R. J. P. Lyon. 1986. Comparison of various techniques for calibration of AIS data. Pages 21-30 in G. Vane and A. F. G. Goetz, editors, *Proceedings -- 2nd Airborne Imaging Spectrometer Data Analysis Workshop*. Jet Propulsion Laboratory Publication 85-35. Jet Propulsion Laboratory, Pasadena, CA.
- Spence, J. R., W. H. Romme, L. Floyd-Hannah, and P. G. Rowlands. 1995. A preliminary vegetation classification for the Colorado Plateau. Pages 193-214 in C. van Riper, editor, *Proceedings -- 2nd Biennial Conference on Research in Colorado Plateau Parks*. National Parks Service Transactions and Proceedings Series NPS/NRNNAU/NRTP-95/11. U.S. Department of Interior, Flagstaff, AZ.
- Trietz, P., and P. Howarth. 2000a. High spatial resolution remote sensing data for forest ecosystem classification: An examination of spatial scale. *Remote Sensing of Environment* 72:268-289.
- Trietz, P., and P. Howarth. 2000b. Integrating spectral, spatial, and terrain variables for forest ecosystem classification. *Photogrammetric Engineering and Remote Sensing* 66:305-317.
- Weber, R. M., and G. A. Dunno. 2001. Riparian vegetation mapping and image processing techniques, Hopi Indian Reservation, Arizona. *Photogrammetric Engineering and Remote Sensing* 67:179-186.
- Woodcock, C. E., A. H. Strahler, and D. L. B. Jupp. 1988a. The use of variograms in remote sensing: I. Scene models and simulated images. *Remote Sensing of Environment* 25:323-348.
- Woodcock, C. E., A. H. Strahler, and D. L. B. Jupp. 1988b. The use of variograms in remote sensing: II. Real digital images. *Remote Sensing of Environment* 25:349-379.

Table 1 ATM band wavelength ranges and calculated signal-to-noise ratios.

Band Number	Wavelength Region	Wavelength Range (micrometers)	Calculated Signal/Noise Ratio (SNR)
1	Blue	0.42-0.44	9.9
2	Blue	0.46-0.51	76.8
3	Green	0.52-0.59	110.2
4	Green/Red	0.59-0.62	129.6
5	Red	0.62-0.67	142.2
6	Red/Near-infrared	0.67-0.72	134.1
7	Near-infrared	0.73-0.85	140.1
8	Near-infrared	0.84-0.97	181.4
9	Short-wave infrared	1.59-1.79	21.2
10	Short-wave infrared	2.10-2.40	30.0
11	Thermal infrared (high gain)	8.28-10.67	16.4
12	Thermal infrared (low gain)	8.28-10.67	21.9

Table 2. Vegetation units mapped by Kearsley and Ayers (2000) at the RM 43.1 site. Both dominant and subordinate species are listed; dominant species are **bold faced**.

Unit	Tree	Shrub	Forbaceous	Herbaceous	Grass	SRFR ¹	
						Series	Association
1	Tamarisk	Snakeweed Brickellbush Fetid marigold	Prince's plume Desert isocoma		Three-awn grass Dropseed grass	02 ISAC (desert isocoma)	GUTI (snakeweed)
2	Tamarisk	Arrowweed	Spiny aster		Dropseed grass	01 TARA (tamarisk)	TESE (arrowweed)
3	Coyote willow Baccharis		Equisetum	Horseweed Cudweed	Canadian wild rye	02 SAEX (coyote willow)	EQFE - BAEM (equisetum-baccharis)
4			Sedge Rush Cattail	Cudweed Plantain	Phragmites Scratchgrass Red top	01 TYDO (cattail)	PHAU (phragmites)
5	Coyote willow		Desert straw Primrose	Dicoria Russian thistle	Desert saltgrass	02 SAEX (coyote willow)	DIBR - SAIB (dicoria-russian thistle)

¹ Classification system devised by Spence et al. (1995).

Table 3. Vegetation units mapped by Kearsley and Ayers (2000) at the RM 51site. Both dominant and subordinate species are listed; dominant species are **bold faced**.

Unit	Tree	Shrub	Forbaceous	Herbaceous	Grass	SRFR ¹	
						Series	Association
1	Coyote willow	Arrowweed	Primrose	Dicoria Russian thistle Tickseed	Dropseed grass	02 SAEX (coyote willow)	DIBR - SAIB (dicoria-russian thistle)
2	Catclaw acacia		Spiny aster		Three-awn grass	05 ACGR (catclaw acacia)	ASSP - ARGL (spiny aster-speedwell)
3	Tamarisk		Desert alyssum		Red brome	01 TARA (tamarisk)	LEFR - BRRU (desert alyssum-red brome)
4	Baccharis Coyote willow		Equisetum	Cudweed Horseweed Spiny sowthistle	Red top	04 SAEX - BAEM (coyote willow & baccharis)	EQFE (equisetum)
5			Rush Cattail Bulrush	Water-cress Plantain	Scratchgrass	01 TYDO (cattail)	JUAR - SCIRPUS (rush-bulrush)

¹ Classification system devised by Spence et al. (1995).

Table 4. Vegetation units mapped by Kearsley and Ayers (2000) at the RM 55.5 site. Both dominant and subordinate species are listed; dominant species are **bold faced**.

Unit	Tree	Shrub	Forbaceous	Herbaceous	Grass	SRFR ¹	
						Series	Association
1				Speedwell	Phragmites Redtop	02 PHAU (phragmites)	AGST (redtop)
2	Tamarisk Baccharis		Climbing milkweed	Clover	Red brome	01 TARA (tamarisk)	BROMUS (red brome)
3	Coyote willow Baccharis	Sagebrush	Equisetum		Scratchgrass	02 SAEX (coyote willow)	BAEM - EQFE (baccharis-equisetum)
4	Mesquite Catclaw acacia	Arrowweed Snakeweed	Desert alyssum		Dropseed grass Rice grass Red brome	06 PRGL (mesquite)	ACGR - TESE (catclaw acacia-arrowweed)
5			Sedge Rush Common three square	Plantain Marsh aster	Scratchgrass	02 CAAQ (sedge)	JUTO - SCIRPUS (rush-bulrush)

¹ Classification system devised by Spence et al. (1995).

Table 5. Vegetation units mapped by Kearsley and Ayers (2000) at the RM 68.2 site. Both dominant and subordinate species are listed; dominant species are **bold faced**..

Unit	Tree	Shrub	Forbaceous	Herbaceous	Grass	SRFR ¹	
						Series	Association
1	Coyote willow Baccharis Tamarisk		Equisetum		Scratchgrass Phragmites Bent grass	04 SAEX - BAEM (coyote willow & baccharis)	EQFE (equisetum)
2	Coyote willow	Arrowweed		Clover	Dropseed grass	02 SAEX (coyote willow)	TESE - SPCR (arrowweed-dropseed grass)
3	Tamarisk	Arrowweed	Camel thorn		Brome grass	01 TARA (tamarisk)	TESE - BROMUS (arrowweed-red brome)
4	Mesquite		Primrose Sand verbena	Dicoria	Dropseed Rice grass	02 GUTI (snakeweed)	ORHY - DIBR (rice grass-dicoria)
5			Cattail Common three square Rush	Goldenrod		01 TYDO (cattail)	JUTO - SOOC (rush-goldenrod)

¹ Classification system devised by Spence et al. (1995).

Table 6. Vegetation units mapped by Kearsley and Ayers (2000) at the RM 71.4 site. Both dominant and subordinate species are listed; dominant species are **bold faced**.

Unit	Tree	Shrub	Forbaceous	Herbaceous	Grass	SRFR ¹	
						Series	Association
1			Bulrush Rush Cattail	Cudweed Clover	Phragmites Red top	02 PHAU (phragmites)	SCIRPUS - JUNCUS (bulrush-rush)
2	Coyote willow Baccharis		Equisetum Goldenrod	Clover	Phragmites Red top	02 SAEX (coyote willow)	BAEM - EQFE (baccharis-equisetum)
3	Tamarisk Mesquite	Arrowweed	Camel thorn Equisetum		Red brome Dropseed grass	01 TESE (Arrowweed)	ALCA - BRRU (camel thorn-red brome)
4	Goodding willow Tamarisk				Red brome	01 SAGO (goodding willow)	TARA - BRRU (tamarisk-red brome)

¹ Classification system devised by Spence et al. (1995).

Table 7. The following list provides the species and genus name for each of the common vegetation names used in the tables, figures, and text in this paper (Phillips et al. 1987).

<u>Common Names</u>	<u>Species/genus</u>	<u>Common Names</u>	<u>Species/genus</u>
Arrowweed	<i>Tessaria sericia</i>	Speedwell	<i>Veronica</i>
Baccharis	<i>Baccharis emoryi</i>	Spiny aster	<i>Aster spinosus</i>
Brickellbush	<i>Brickellia longifolia</i>	Spiny sowthistle	<i>Sonchus asper</i>
Bulrush	<i>Scirpus</i>	Tamarisk	<i>Tamarix pentandra</i>
Camel thorn	<i>Alhagi camelorum</i>	Three-awn grass	<i>Aristida glauca</i>
Canadian wild rye	<i>Elymus canadensis</i>	Tickseed	<i>Corispermum nitidum</i>
Catclaw acacia	<i>Acacia greggii</i>	Water-cress	<i>Nasturtium officinale</i>
Cattail	<i>Typha domingensis</i>	White brittlebush	<i>Encelia farinosa</i>
Climbing milkweed	<i>Sarcostemma cynanchoides</i>		
Clover	<i>Melilotus</i>		
Common three square	<i>Scirpus pungens</i>		
Coyote willow	<i>Salix exigua</i>		
Cudweed	<i>Gnaphalium chilense</i>		
Desert alyssum	<i>Lepidium fremontii</i>		
Desert isocoma	<i>Isocoma acradenia</i>		
Desert saltgrass	<i>Distichilis spicata</i>		
Desert straw	<i>Stephanomeria pauciflora</i>		
Dicoria	<i>Dicoria brandegei</i>		
Dropseed grass	<i>Sporobolus flexuosus, cryptandrus</i>		
Equisetum	<i>Equisetum</i>		
Fetid marigold	<i>Dyssodia pentachaeta</i>		
Goldenrod	<i>Solidago occidentalis</i>		
Goodding willow	<i>Salix gooddingii</i>		
Horseweed	<i>Conyza canadensis</i>		
March aster	<i>Aster subulatus</i>		
Mesquite	<i>Prosopis glandulosa</i>		
Phragmites	<i>Phragmites australis</i>		
Plantain	<i>Plantago major</i>		
Primrose	<i>Oenothera pallida</i>		
Prince's plum	<i>Stanleya pinnata</i>		
Red brome	<i>Bromus rubens</i>		
Red top	<i>Agrostis stolonifera</i>		
Rice grass	<i>Oryzopsis hymenoides</i>		
Rush	<i>Juncus, Juncus torryi</i>		
Russian thistle	<i>Salsola iberica</i>		
Sagebrush	<i>Artemesia ludoviciana</i>		
Sand verbena	<i>Abronia elliptica</i>		
Scratch grass	<i>Muhlenbergia asperifolia</i>		
Sedge	<i>Carex aquatilis</i>		
Snakeweed	<i>Gutierrezia</i>		

Table 8. Classification producer accuracies for overall site and individual vegetation units at each study site derived from maximum likelihood classification of spectral band reflectance and texture. Overall site producer accuracies also provided for separate analyses using only the spectral bands.

River Mile Study Site and Vegetation Unit	SRFR ¹ Vegetation Series	SRFR ¹ Vegetation Association	Film CIR 11 cm 07/00	Film CIR 28 cm 09/00	Film CIR 30.5 cm 03/00	Emerge CIR 30.5 cm 09/99	Bechtel ATM 100 cm 07/00
RM 43.1							
Unit 1	Desert isocoma	Snakeweed	3.5	13.9	0.2	15.6	10.9
Unit 2	Tamarisk	Arrowweed	79.0	69.5	51.2	40.0	71.4
Unit 3	Coyote willow	Equisetum-Baccharis	72.6	19.3	53.9	68.6	51.6
Unit 4	Cattail	Phragmites	74.5	53.0	75.0	31.0	70.0
Unit 5	Coyote willow	Dicoria-russian thistle	1.0	3.0	0.0	21.1	28.2
<i>Overall accuracy using spectral & texture data</i>			<i>69.1</i>	<i>36.0</i>	<i>51.0</i>	<i>51.8</i>	<i>53.9</i>
<i>Overall accuracy using spectral data</i>			<i>59.3</i>	<i>38.7</i>	<i>45.2</i>	<i>47.5</i>	<i>53.9</i>
RM 51							
Unit 1	Coyote willow	Dicoria-russian thistle	36.7			56.5	43.5
Unit 2	Catchlaw acacia	Spiny aster-speedwell	6.4			13.5	71.4
Unit 3	Tamarisk	Desert alyssum-red brome	75.7			62.8	70.5
Unit 4	Coyote willow-Baccharis	Equisetum	30.7			50.0	32.4
Unit 5	Cattail	Rush-bulrush	57.0			68.0	71.7
<i>Overall accuracy using spectral & texture data</i>			<i>57.1</i>			<i>55.5</i>	<i>62.1</i>
<i>Overall accuracy using spectral data</i>			<i>52.4</i>			<i>53.5</i>	<i>61.1</i>
RM 55.5							
Unit 1	Phragmites	Redtop	42.5			38.9	64.4
Unit 2	Tamarisk	Red brome	70.9			54.8	47.3

River Mile Study Site and Vegetation Unit	SRFR ¹ Vegetation Series	SRFR ¹ Vegetation Association	Film CIR 11 cm 07/00	Film CIR 28 cm 09/00	Film CIR 30.5 cm 03/00	Emerge CIR 30.5 cm 09/99	Bechtel ATM 100 cm 07/00
Unit 3	Coyote willow	Baccharis-equisetum	41.8			44.4	64.1
Unit 4	Mesquite	Catclaw acacia-arrowweed	68.9			55.5	66.9
Unit 5	Sedge	Rush-bulrush	13.8			30.2	57.7
<i>Overall accuracy using spectral & texture data</i>			56.7			48.8	54.8
<i>Overall accuracy using spectral data</i>			37.1			44.8	52.4
RM 68.2							
Unit 1	Coyote willow-Baccharis	Equisetum	62.9	67.4	27.7	54.2	69.1
Unit 2	Coyote willow	Arrowweed-dropseed grass	46.9	41.7	21.8	17.0	53.3
Unit 3	Tamarisk	Arrowweed-red brome	70.3	56.9	81.3	78.6	72.8
Unit 4	Snakeweed	Rice grass-dicoria	72.6	64.2	65.6	67.8	70.5
Unit 5	Cattail	Rush-goldenrod	3.1	18.5	32.6	16.9	21.9
<i>Overall accuracy using spectral & texture data</i>			62.6	58.0	53.8	59.2	67.0
<i>Overall accuracy using spectral data</i>			43.4	40.2	55.0	57.8	62.7
RM 71.4							
Unit 1	Phragmites	Bulrush-rush	49.7			37.4	58.7
Unit 2	Coyote willow	Baccharis-equisetum	49.6			47.3	61.7
Unit 3	Arrowweed	Camel thorn-red brome	55.0			39.4	75.3
Unit 4	Goodding willow	Tamarisk-red brome	93.4			74.1	90.8
<i>Overall accuracy using spectral & texture data</i>			71.0			56.3	78.1
<i>Overall accuracy using spectral data</i>			40.2			48.2	75.7

¹Classification system of Spence et al. (1994).

Table 9. Vegetation unit producer accuracies and overall site producer accuracies from maximum likelihood classification results using various ATM band combinations and from scanned-film CIR data. Unit accuracies that are 10% lower than those obtained using the full ATM database are indicated as **bold-faced** values.

River Mile Study Site and Vegetation Unit	SRFR ¹ Vegetation Series	SRFR ¹ Vegetation Association	Film CIR 11 cm 07/00	Bechtel ATM bands 3, 6, 7	Bechtel ATM bands 3, 4, 6, 7	Bechtel ATM bands 3, 4, 6, 7, 10	Nine Bechtel ATM bands
RM 43.1							
Unit 1	Desert isocoma	Snakeweed	3.5	12.7	14.6	7.4	10.9
Unit 2	Tamarisk	Arrowweed	79.0	59.4	63.1	65.7	71.4
Unit 3	Coyote willow	Equisetum-Baccharis	72.6	46.8	53.2	59.6	51.6
Unit 4	Cattail	Phragmites	74.5	53.4	66.2	62.4	70.0
Unit 5	Coyote willow	Dicoria-russian thistle	1.0	45.2	40.6	27.4	28.2
<i>Overall</i>			<i>69.1</i>	<i>47.8</i>	<i>52.1</i>	<i>55.2</i>	<i>53.9</i>
RM 51							
Unit 1	Coyote willow	Dicoria-russian thistle	36.7	40.6	39.5	45.5	43.5
Unit 2	Catclaw acacia	Spiny aster-speedwell	6.4	50.7	68.7	64.0	71.4
Unit 3	Tamarisk	Desert alyssum-red brome	75.7	68.2	66.1	69.4	70.5
Unit 4	Coyote willow-Baccharis	Equisetum	30.7	27.1	22.8	28.9	32.4
Unit 5	Cattail	Rush-bulrush	57.0	62.2	61.6	67.3	71.7
<i>Overall</i>			<i>57.1</i>	<i>56.9</i>	<i>56.8</i>	<i>59.8</i>	<i>62.1</i>
RM 55.5							
Unit 1	Phragmites	Red top	42.5	53.9	56.5	62.0	64.4
Unit 2	Tamarisk	Red brome	70.9	45.3	45.8	45.8	47.3
Unit 3	Coyote willow	Baccharis-equisetum	41.8	57.7	58.4	63.3	64.1
Unit 4	Mesquite	Catclaw acacia-arrowweed	68.9	58.7	58.3	66.2	66.9

River Mile Study Site and Vegetation Unit	SRFR ¹ Vegetation Series	SRFR ¹ Vegetation Association	Film CIR 11 cm 07/00	Bechtel ATM bands 3, 6, 7	Bechtel ATM bands 3, 4, 6, 7	Bechtel ATM bands 3, 4, 6, 7, 10	Nine Bechtel ATM bands
Unit 5	Sedge	Rush-bulrush	13.8	52.9	52.7	56.9	57.7
<i>Overall</i>			<i>56.7</i>	<i>51.4</i>	<i>51.9</i>	<i>53.3</i>	<i>54.8</i>
RM 68.2							
Unit 1	Coyote willow-Baccharis	Equisetum	62.9	57.0	57.7	70.2	69.1
Unit 2	Coyote willow	Arrowweed-dropseed grass	46.9	45.7	48.7	46.5	53.3
Unit 3	Tamarisk	Arrowweed-red brome	70.3	60.4	68.2	71.3	72.8
Unit 4	Snakeweed	Rice grass-dicoria	72.6	71.3	67.2	68.0	70.5
Unit 5	Cattail	Rush-goldenrod	3.1	25.3	23.4	22.9	21.9
<i>Overall</i>			<i>62.6</i>	<i>57.1</i>	<i>60.7</i>	<i>65.7</i>	<i>67.0</i>
RM 71.4							
Unit 1	Phragmites	Bulrush-rush	49.7	47.4	50.0	51.0	58.7
Unit 2	Coyote willow	Baccharis-equisetum	54.1	54.1	56.4	56.8	61.7
Unit 3	Arrowweed	Camel thorn-red brome	55.0	73.7	74.1	76.2	75.3
Unit 4	Goodding willow	Tamarisk-red brome	93.4	84.4	86.6	87.9	90.8
<i>Overall</i>			<i>71.0</i>	<i>72.4</i>	<i>74.1</i>	<i>75.4</i>	<i>78.1</i>

¹ Classification system of Spence et al. (1994).

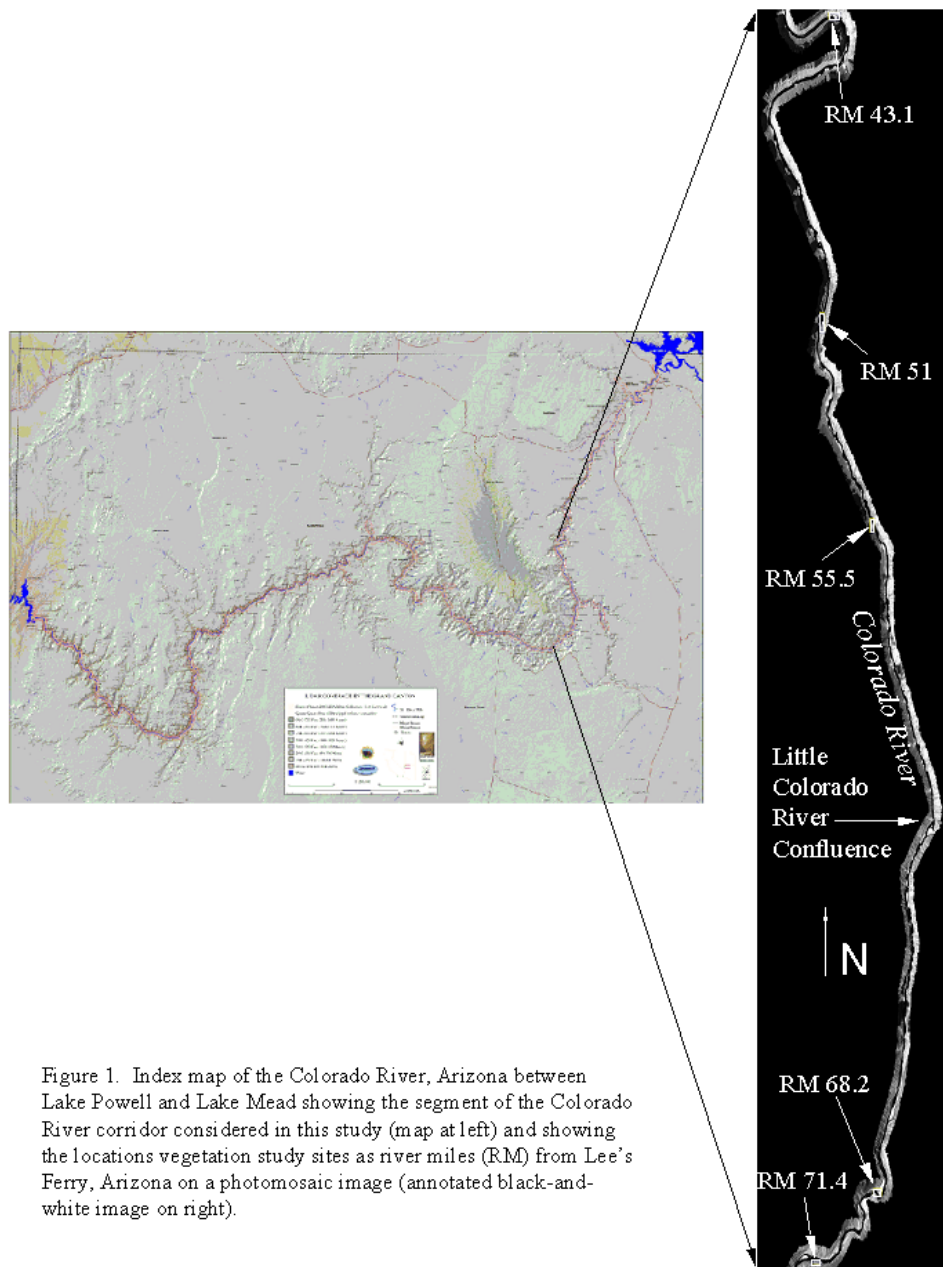


Figure 1. Index map of the Colorado River, Arizona between Lake Powell and Lake Mead showing the segment of the Colorado River corridor considered in this study (map at left) and showing the locations vegetation study sites as river miles (RM) from Lee's Ferry, Arizona on a photomosaic image (annotated black-and-white image on right).

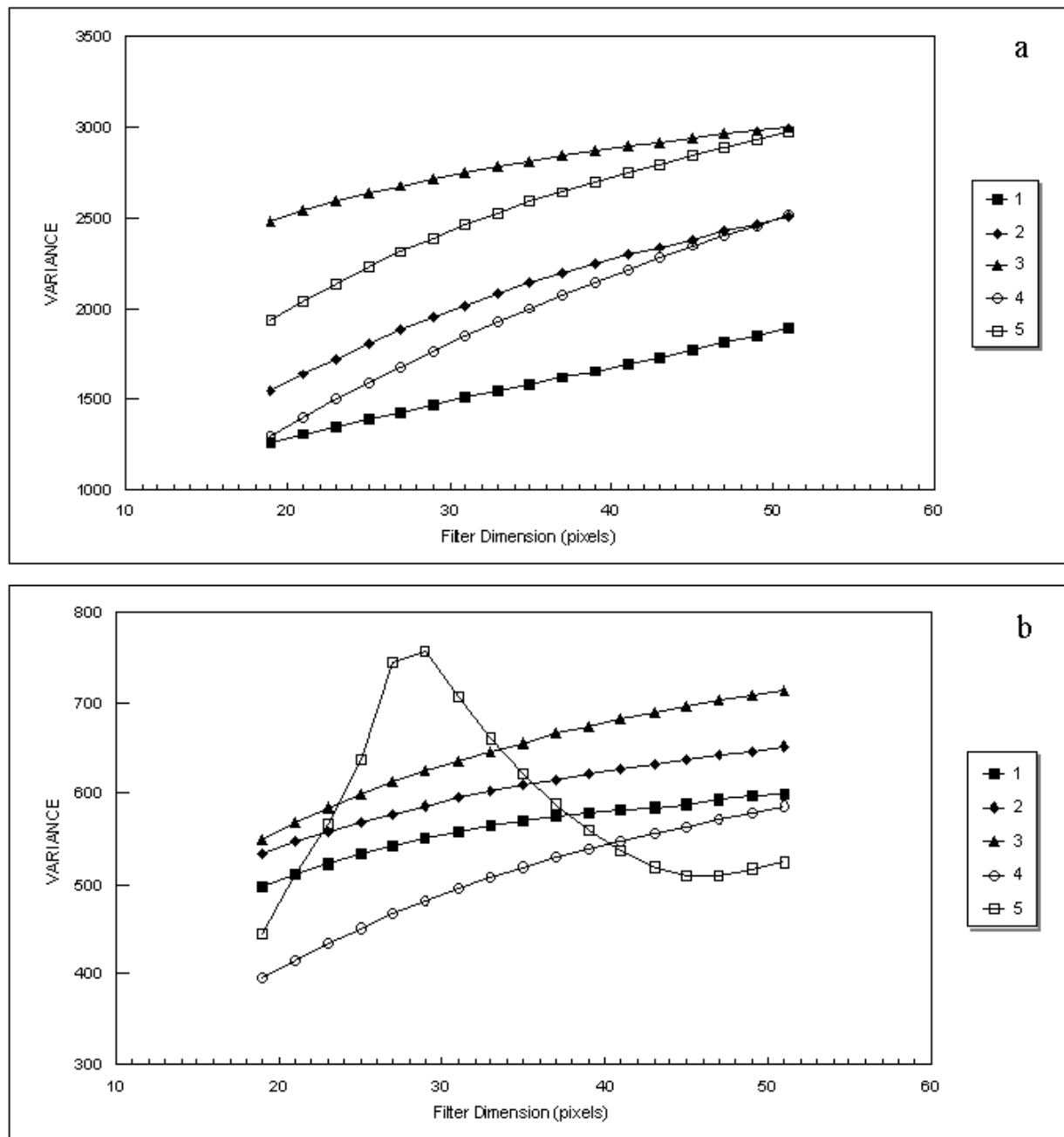


Figure 2. Variations in average variance within and between vegetation units relative to the dimension of the variance filter at (a) study site RM 68.2 using the September, 2000 28-cm CIR image data, and (b) study site RM 43.1 using the March, 2000 30.5-cm CIR image data.

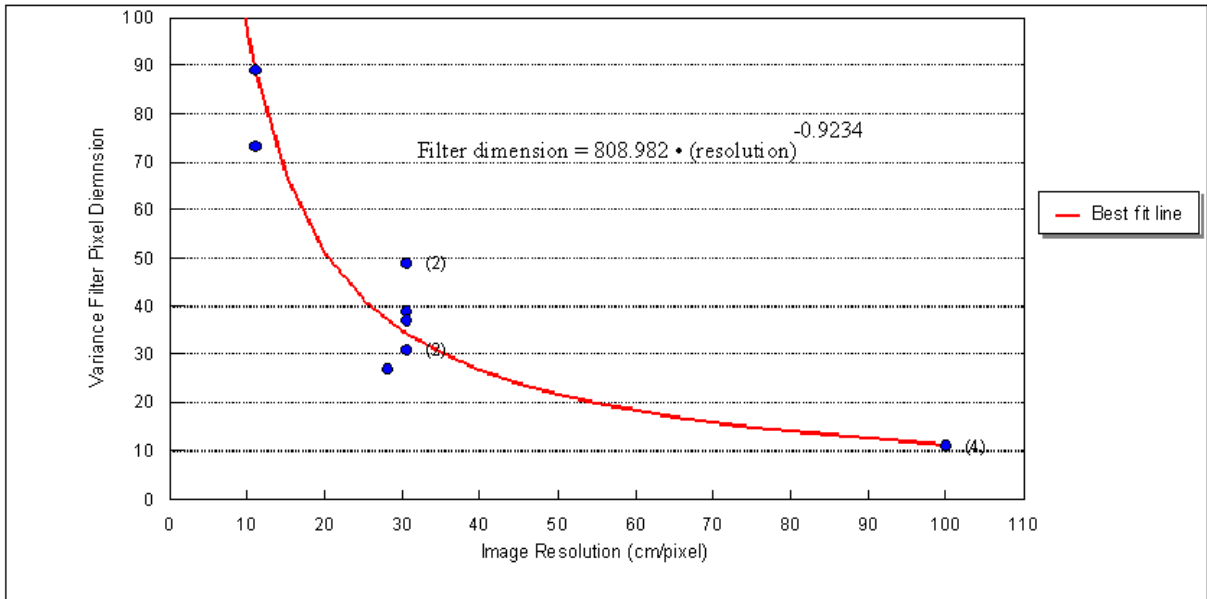


Figure 3. Plot of variance filter dimension for optimum separation of vegetation units within the five study areas as a function of image resolution. Best line derived from least squares analysis of data points. Equation shown is the least-squares solution to a power law, which produced the highest correlation coefficient (0.933). Values in parentheses are the number of coincident data points at an x,y location.

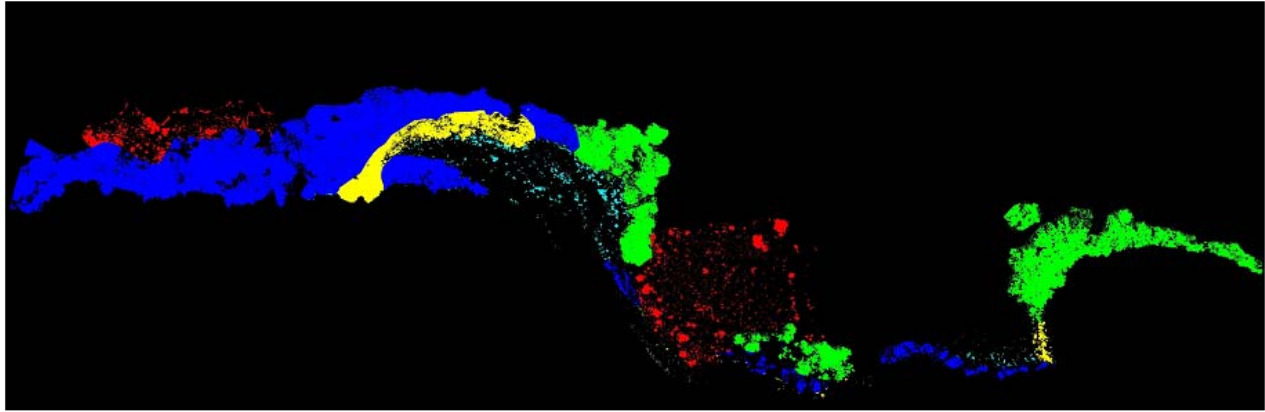


Figure 4. Vegetation map of study site RM43.1 produced from field observations by Kearsley and Ayers (2000). Map excludes bare ground.

	Vegetation Series	Vegetation Association
1	Desert isocoma	snakeweed
2	Tamarisk	arrowweed
3	Coyote willow	equisetum, baccharis
4	Cattail	phragmites
5	Coyote willow	dicoria, russian thistle

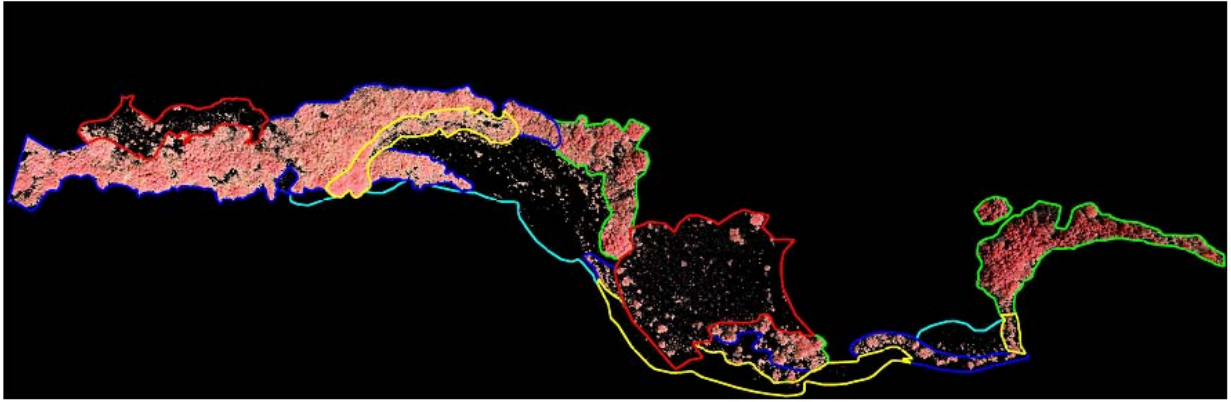


Figure 5. Vegetation unit outlines superposed on CIR image of study site RM43.1.

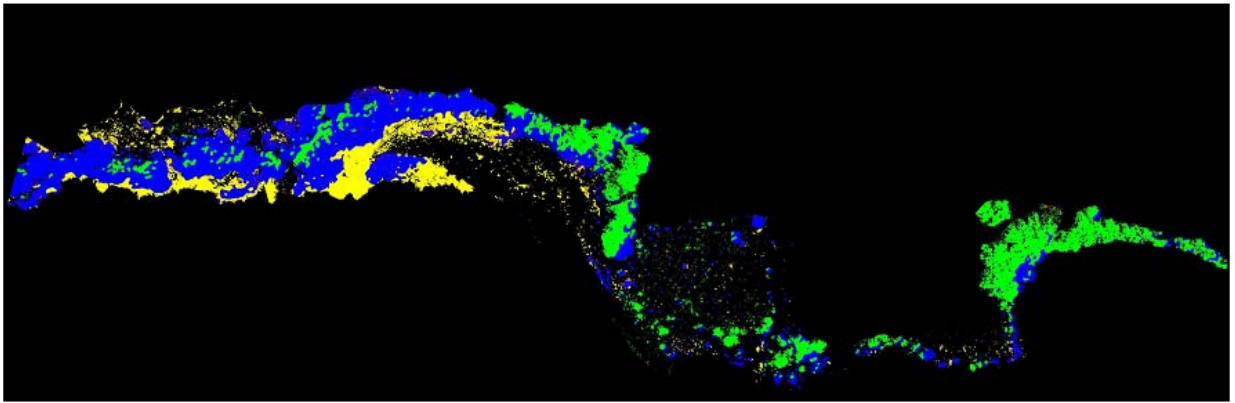


Figure 6. Vegetation classification map of study site RM43.1 produced using maximum likelihood classifier on July, 2000 11-cm CIR band data and texture data. Map excludes bare ground.

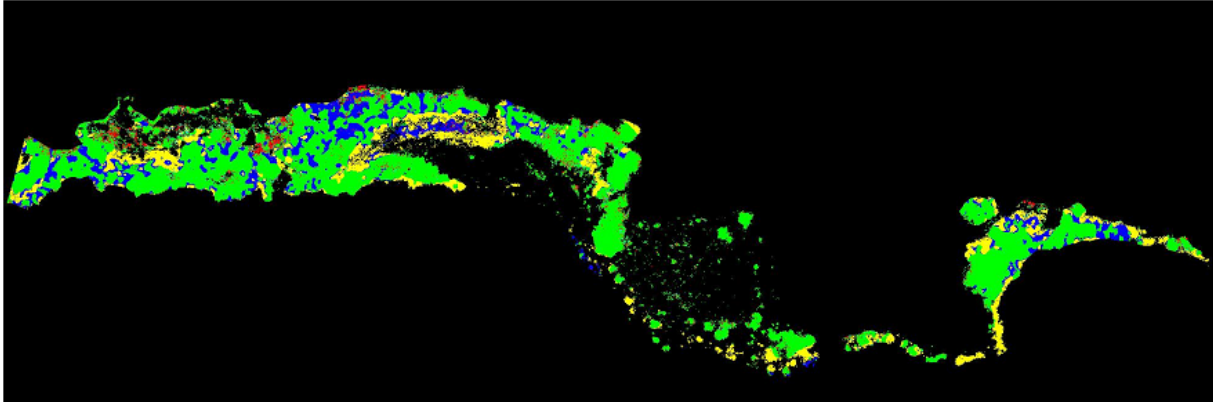


Figure 7. Vegetation classification map of study site RM43.1 produced using maximum likelihood classifier on September, 2000 28-cm CIR band data and texture data. Map excludes bare ground.

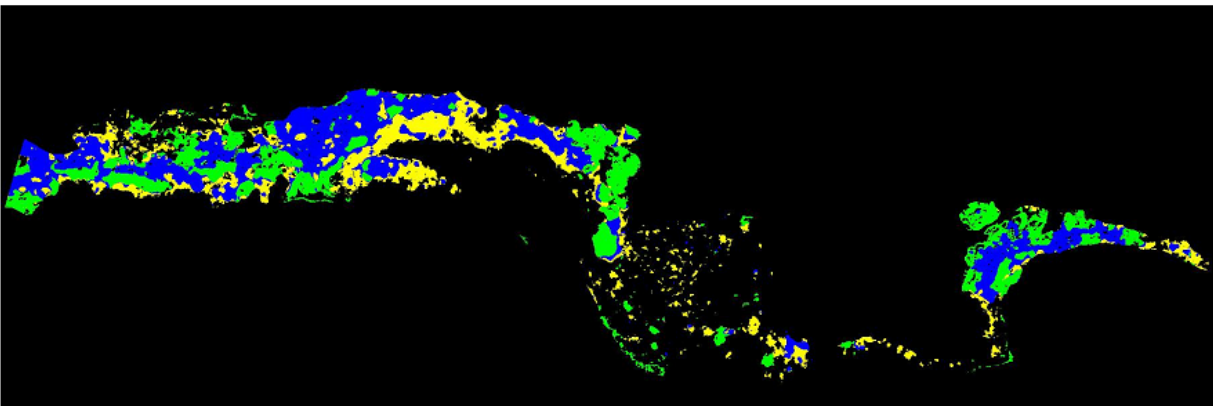


Figure 8. Vegetation classification map of study site RM43.1 produced using maximum likelihood classifier on March, 2000 30.5-cm CIR band data and texture data. Map excludes bare ground.

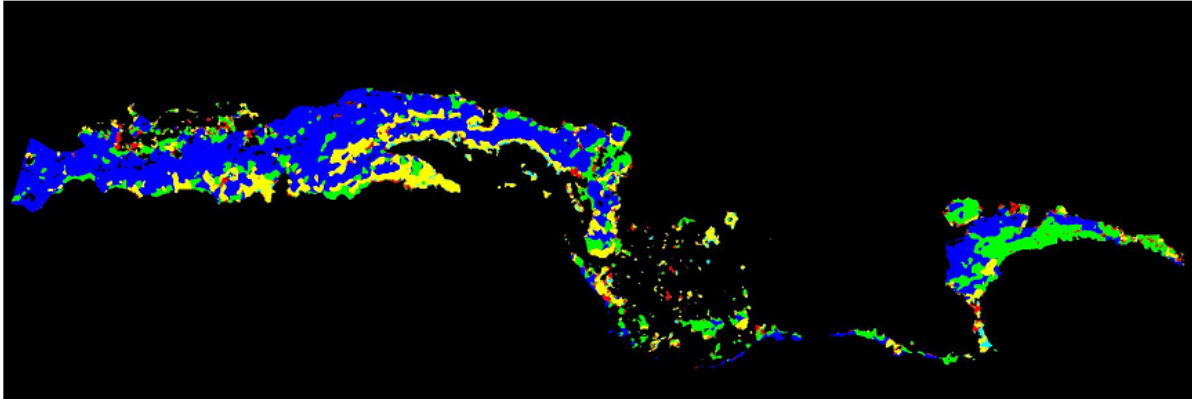


Figure 9. Vegetation classification map of study site RM43.1 produced using maximum likelihood classifier on September, 1999 30.5-cm Emerge CIR band data and texture data. Map excludes bare ground.

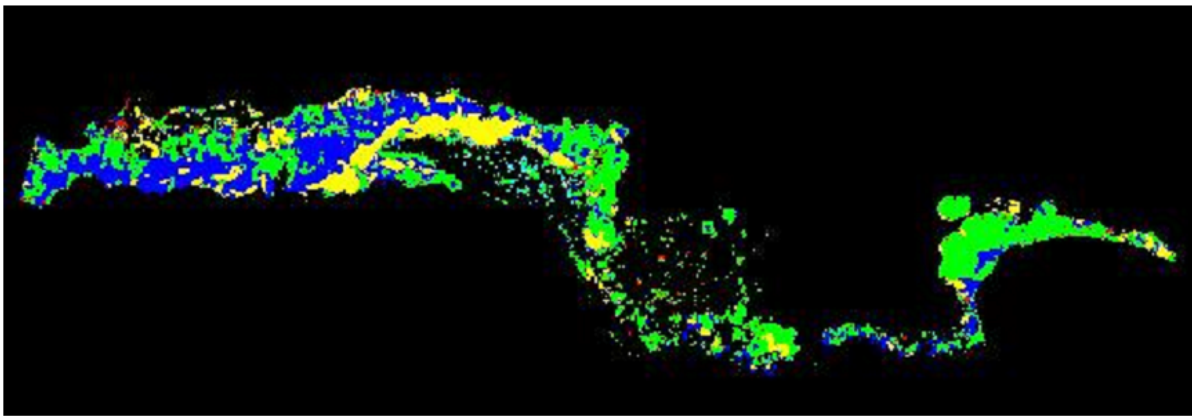


Figure 10. Vegetation classification map of study site RM43.1 produced using maximum likelihood classifier on July, 2000 100-cm ATM band data and texture data. Map excludes bare ground.

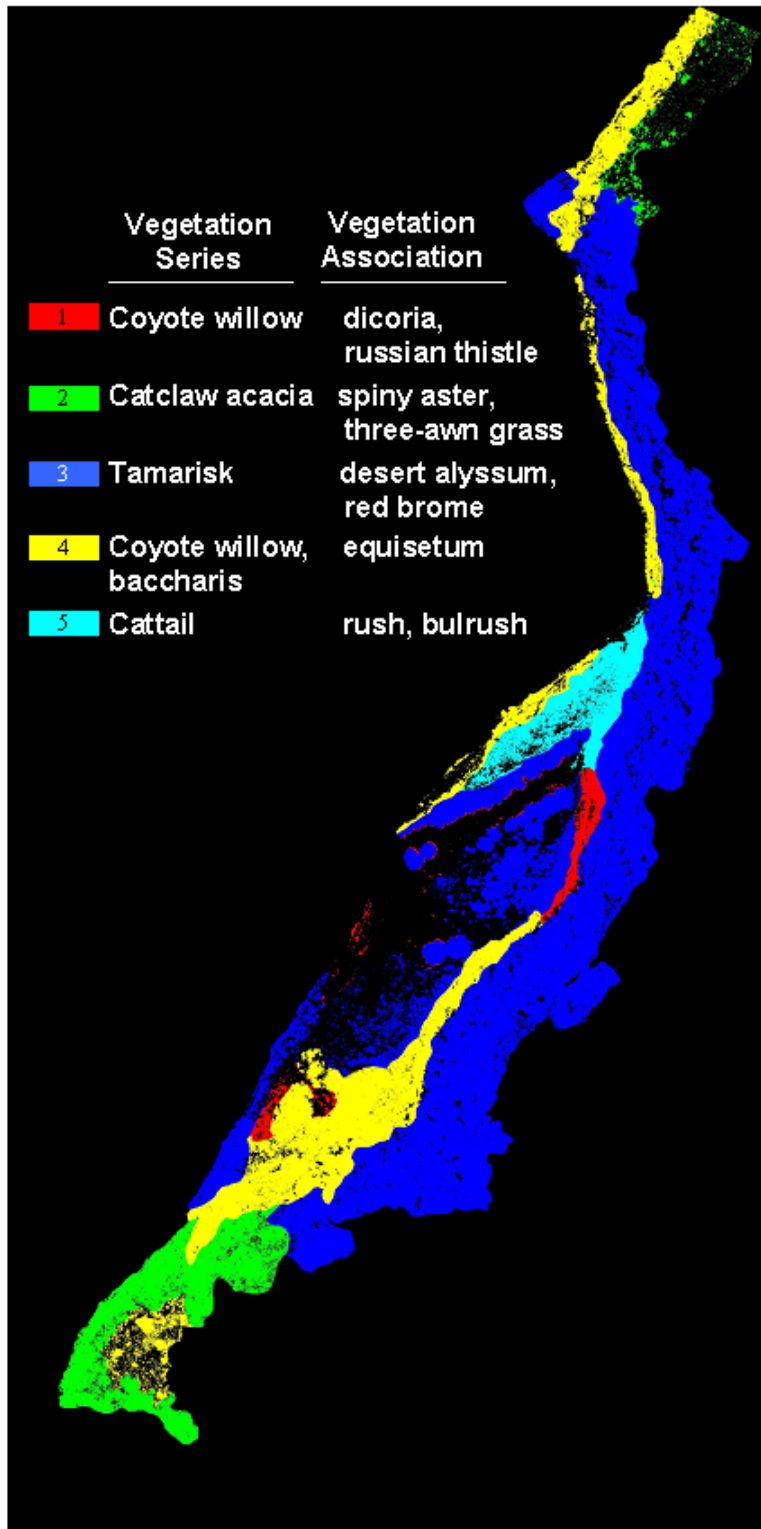


Figure 11. Vegetation map of study site RM51 produced from field observations by Kearsley and Ayers (2000). Map excludes bare ground.

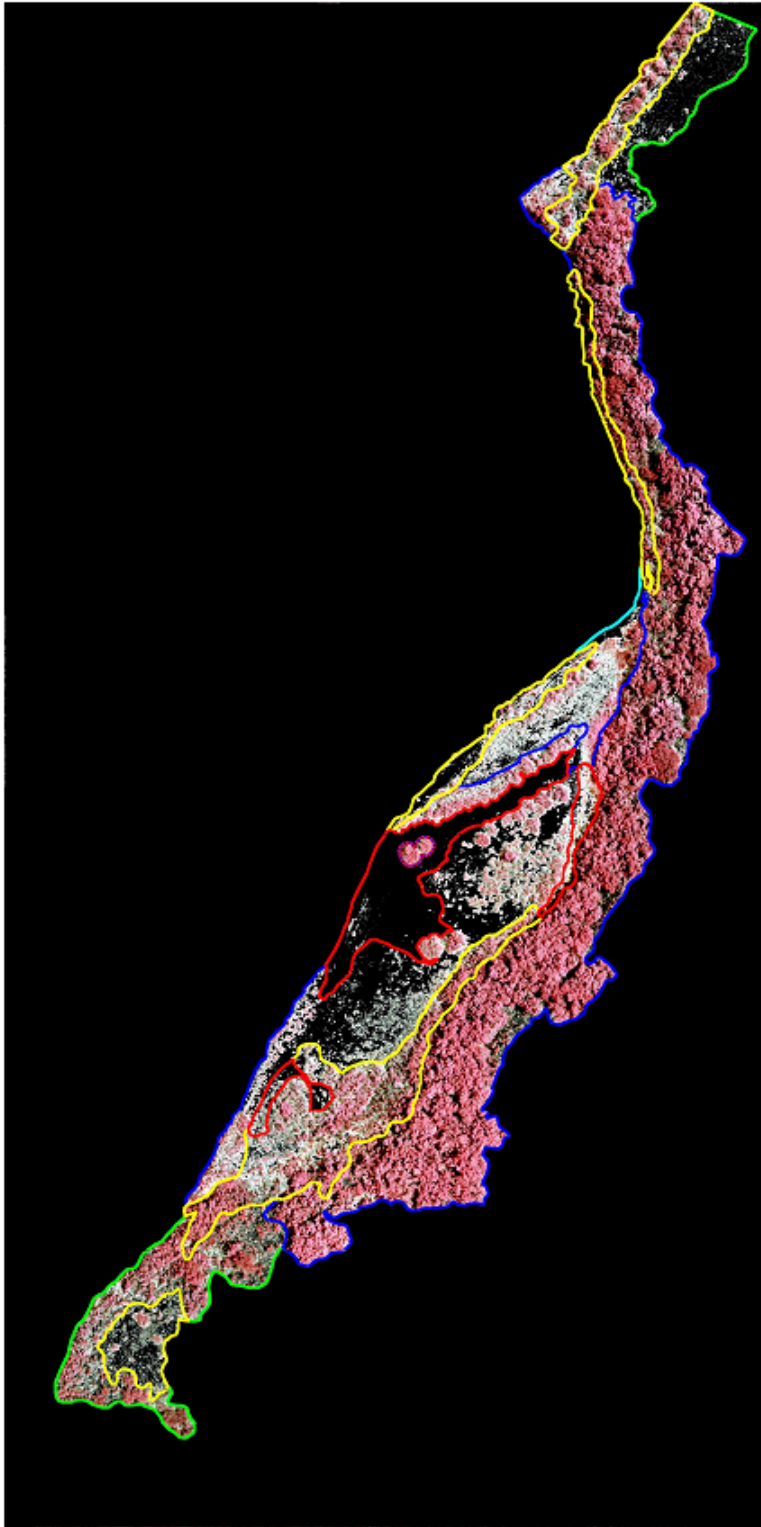


Figure 12. Vegetation unit outlines superposed on CIR image of study site RM51.

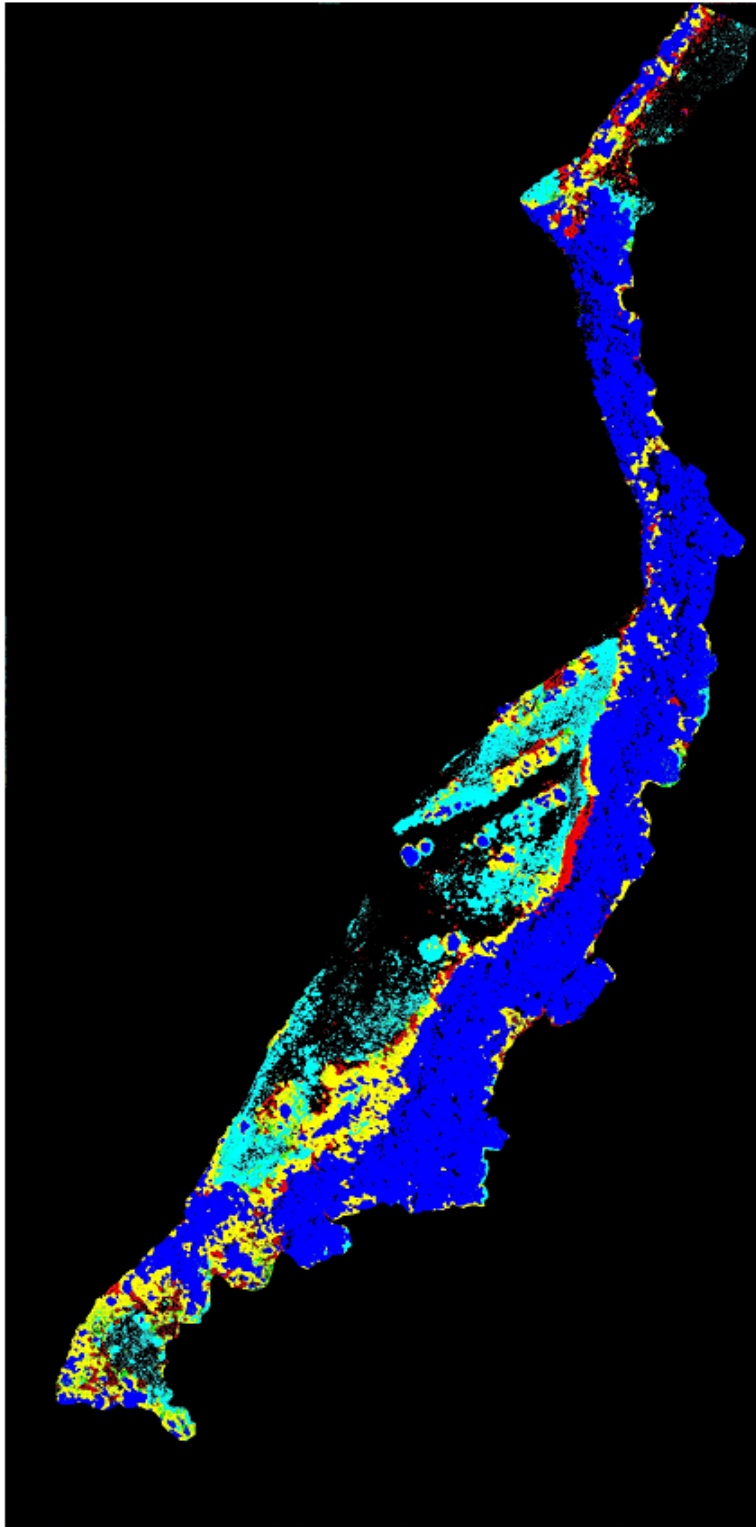


Figure 13. Vegetation classification map of study site RM51 produced using maximum likelihood classifier on July, 2000 11-cm CIR band data and texture data. Map excludes bare ground.

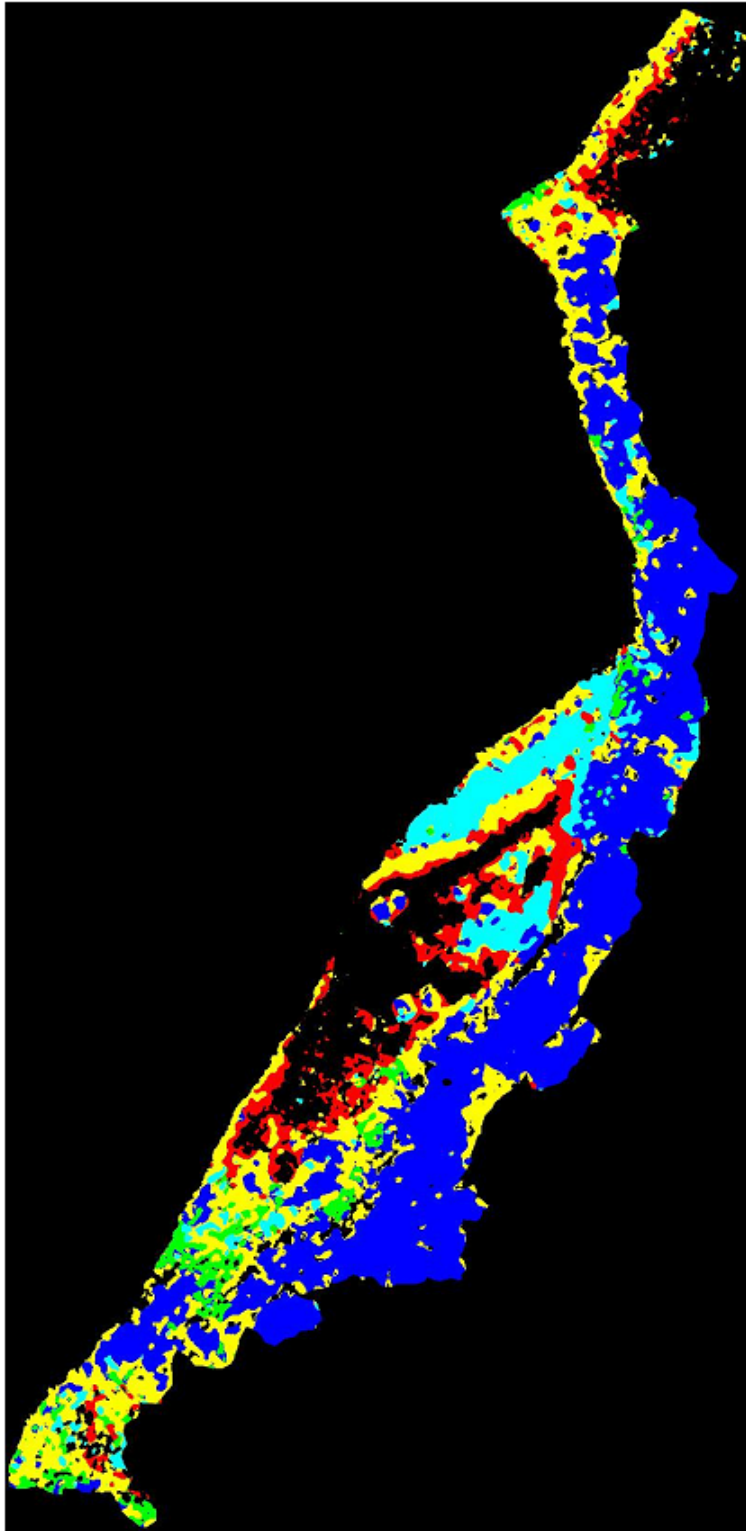


Figure 14. Vegetation classification map of study site RM51 produced using maximum likelihood classifier on September, 1999 30.5-cm Emerge CIR band data and texture data. Map excludes bare ground.

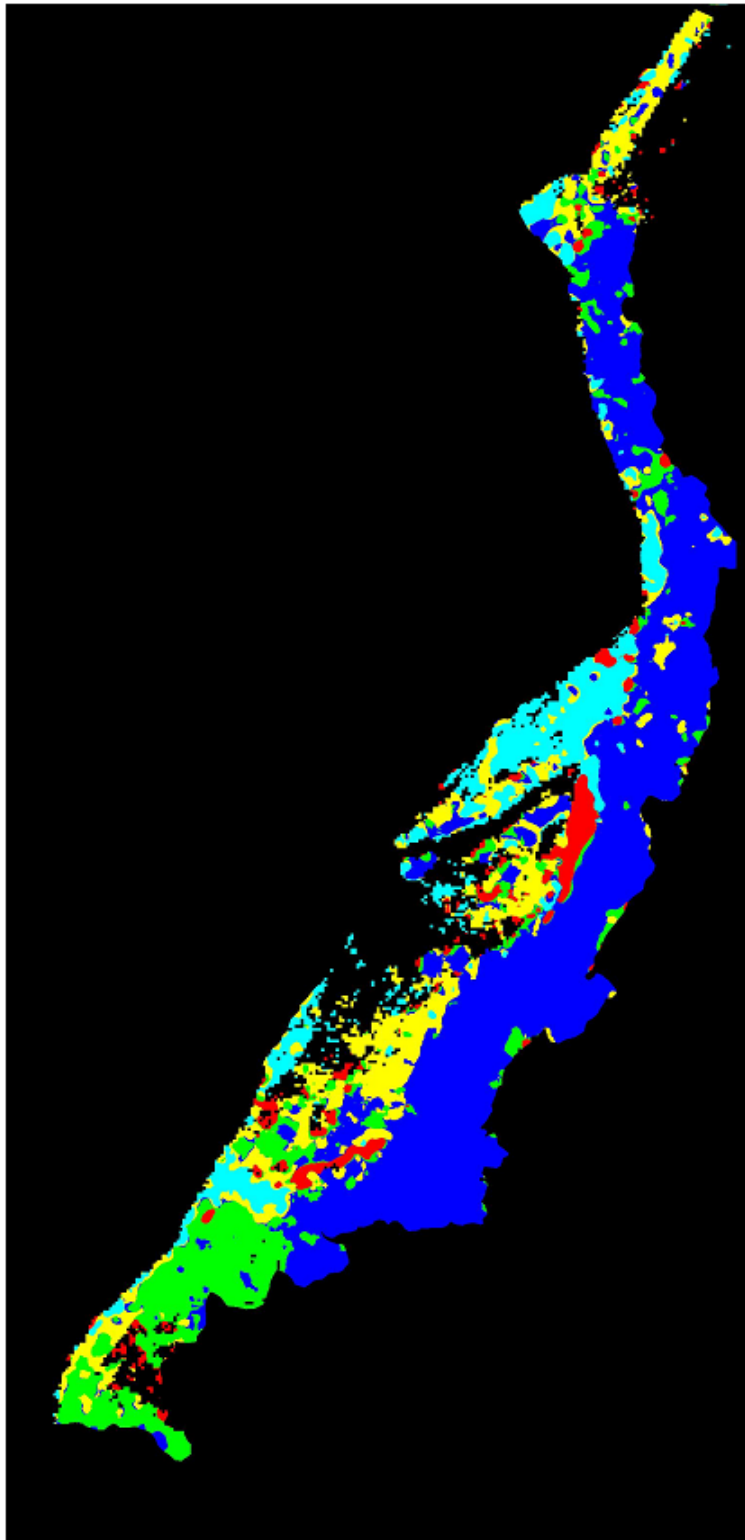


Figure 15. Vegetation classification map of study site RM51 produced using maximum likelihood classifier on July, 2000 100-cm ATM band data and texture data. Map excludes bare ground.

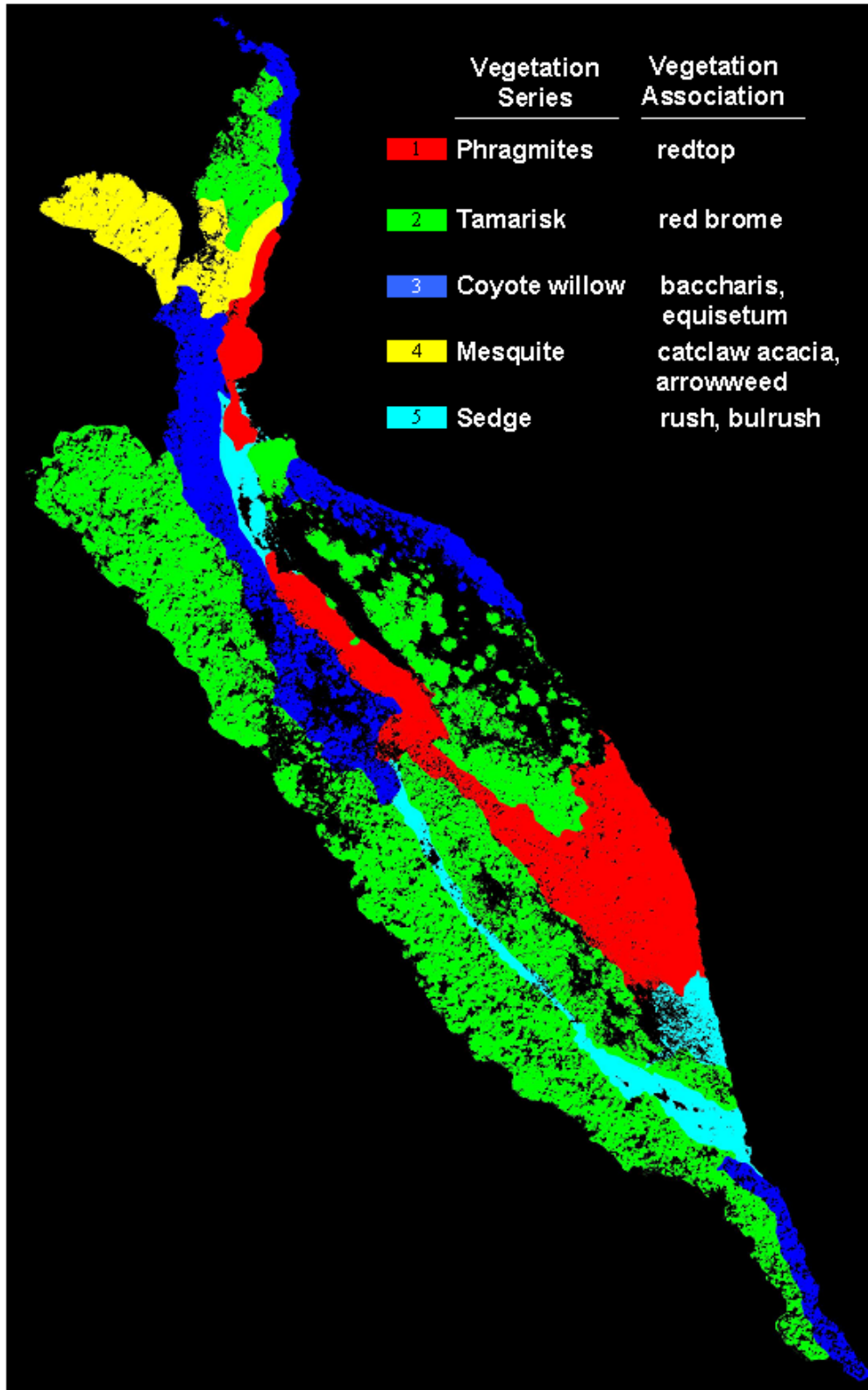


Figure 16. Vegetation map of study site RM55.5 produced from field observations by Kearsley and Ayers (2000). Map excludes bare ground.

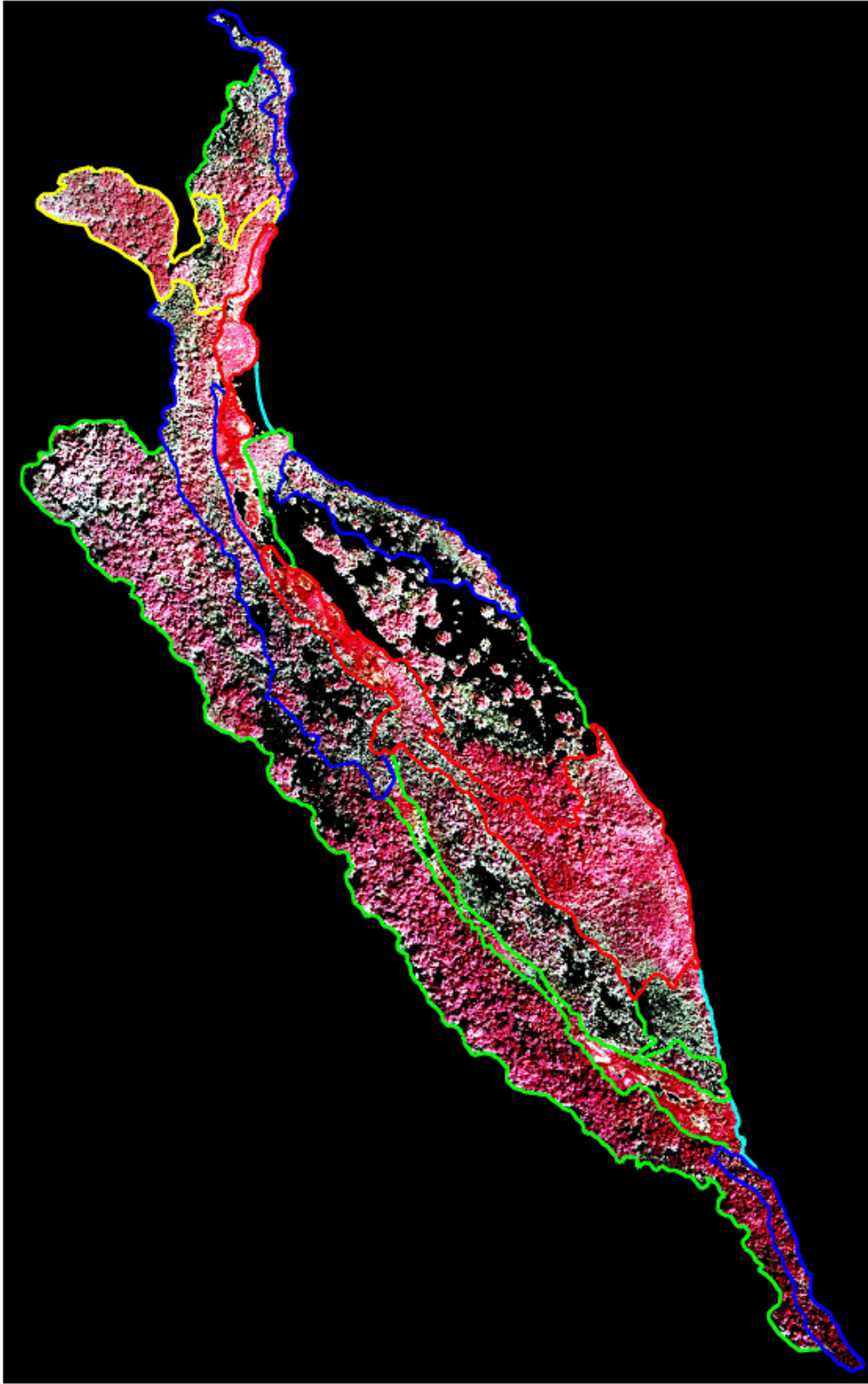


Figure 17. Vegetation unit outlines superposed on CIR image of study site RM55.5.

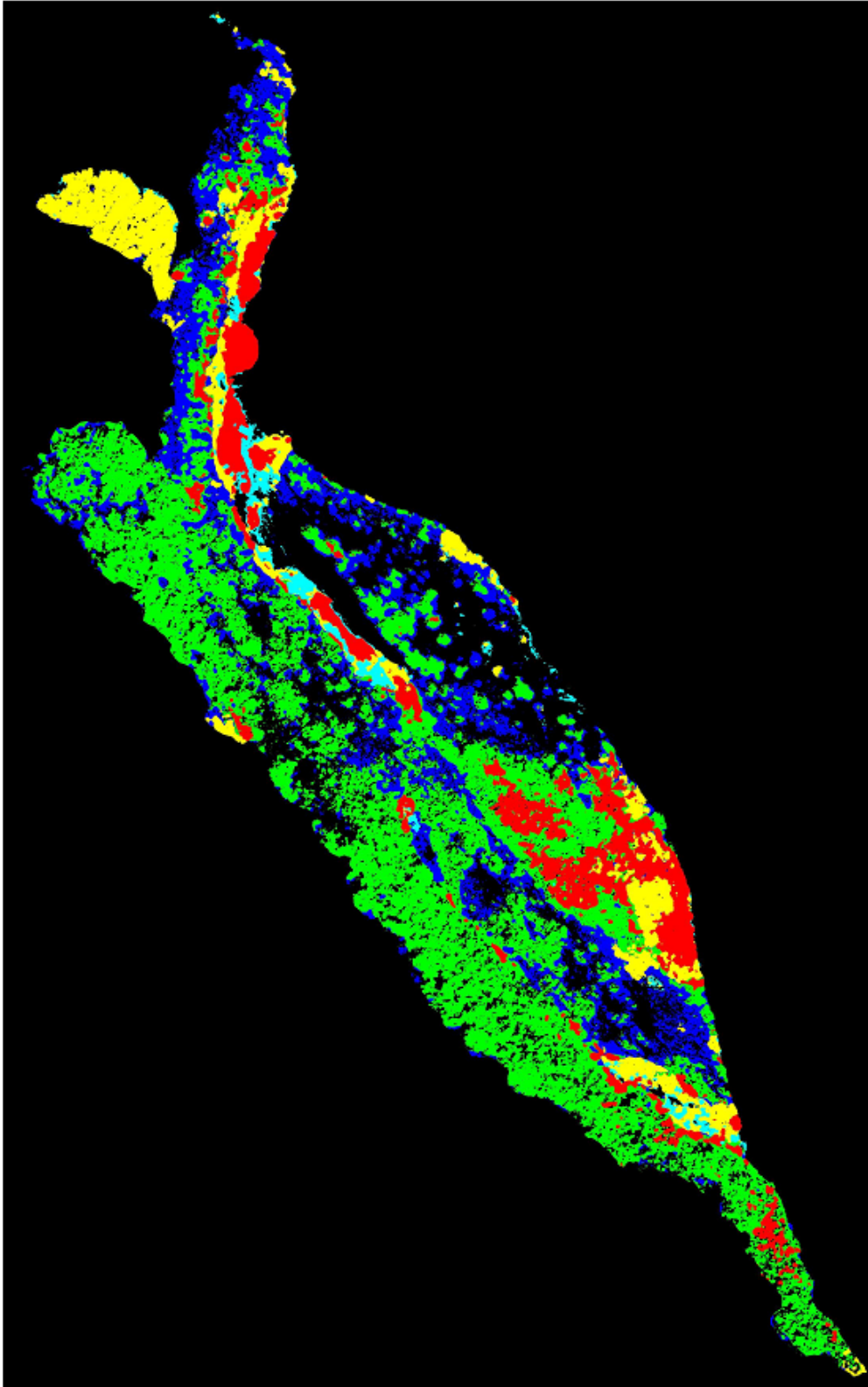


Figure 18. Vegetation classification map of study site RM55.5 produced using maximum likelihood classifier on July, 2000 11-cm CIR band data and texture data. Map excludes bare ground.

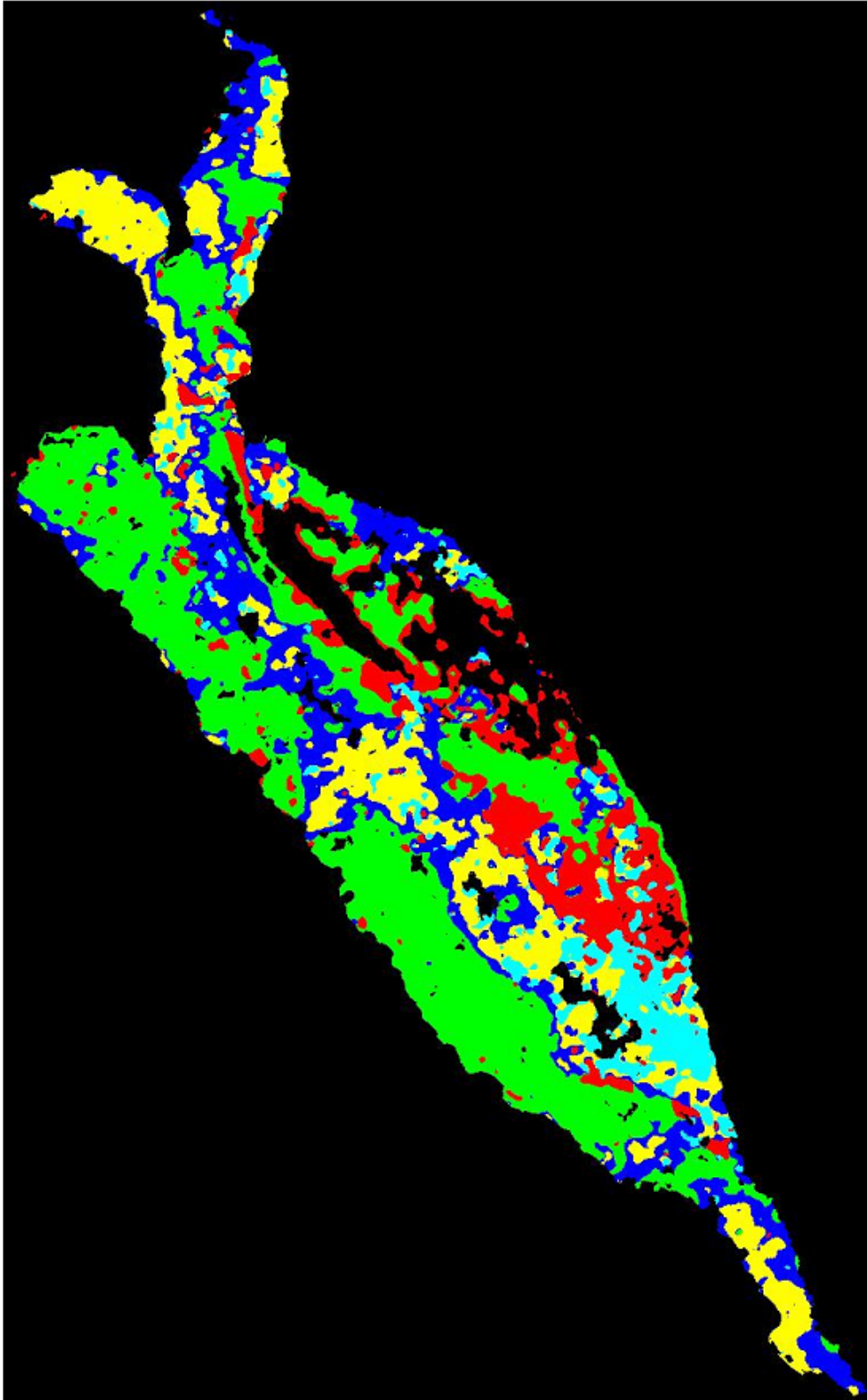


Figure 19. Vegetation classification map of study site RM55.5 produced using maximum likelihood classifier on September, 1999 30.5-cm Emerge CIR band data and texture data. Map excludes bare ground.

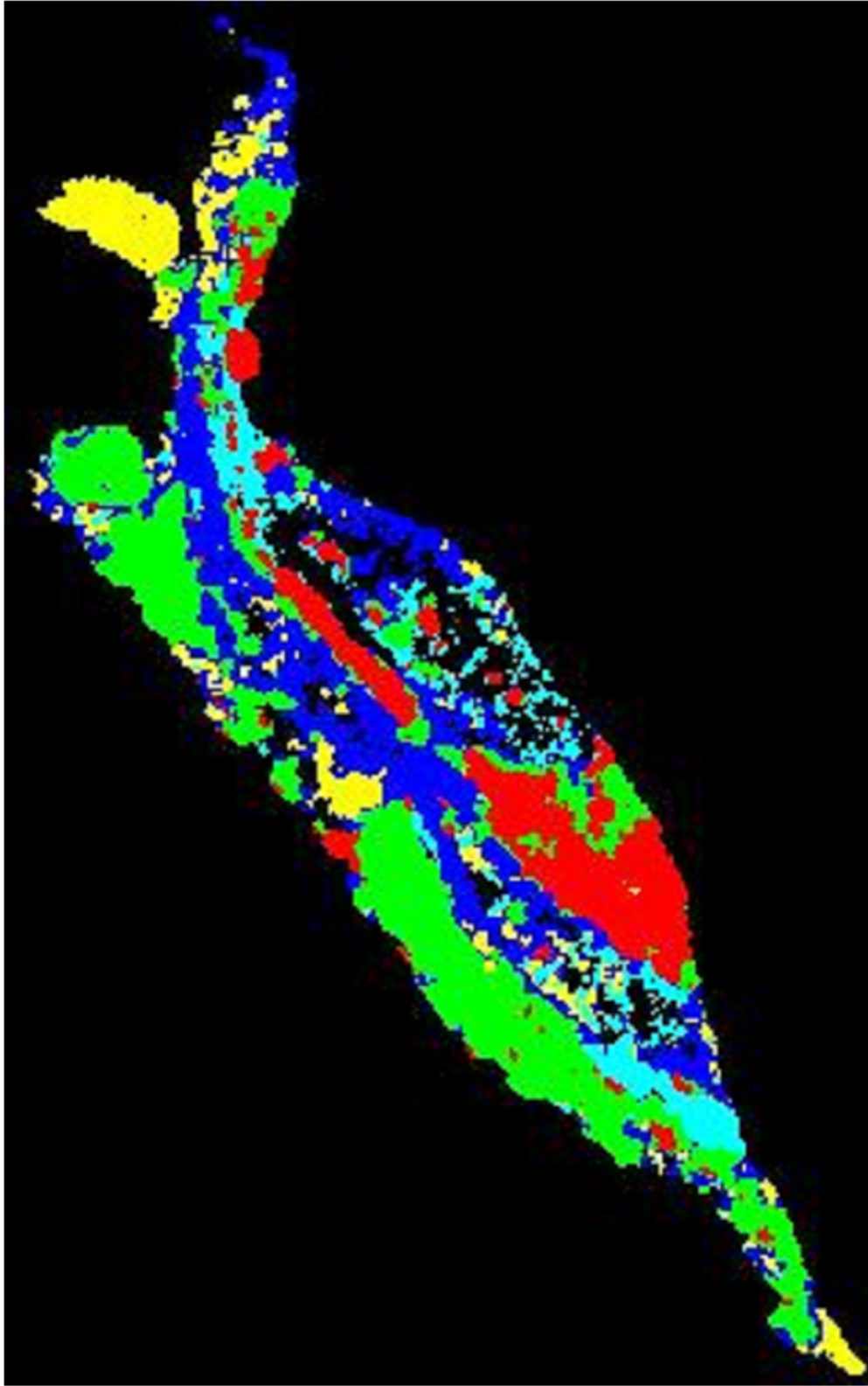


Figure 20. Vegetation classification map of study site RM55.5 produced using maximum likelihood classifier on July, 2000 100-cm ATM band data and texture data. Map excludes bare ground.

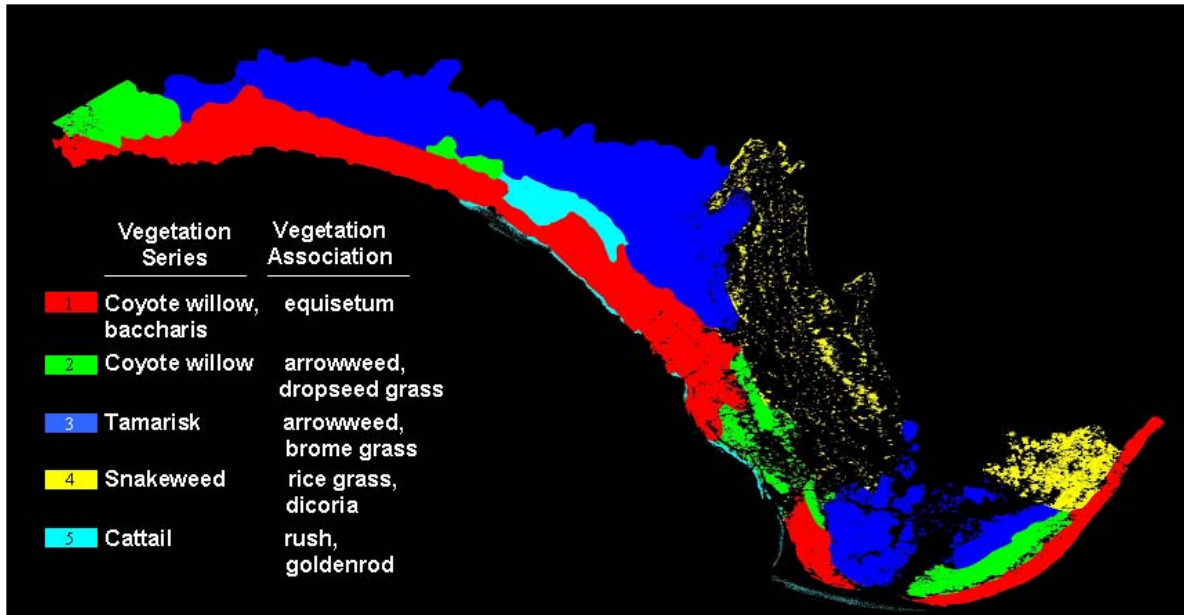


Figure 21. Vegetation map of study site RM68.2 produced from field observations by Kearsley and Ayers (2000). Map excludes bare ground.

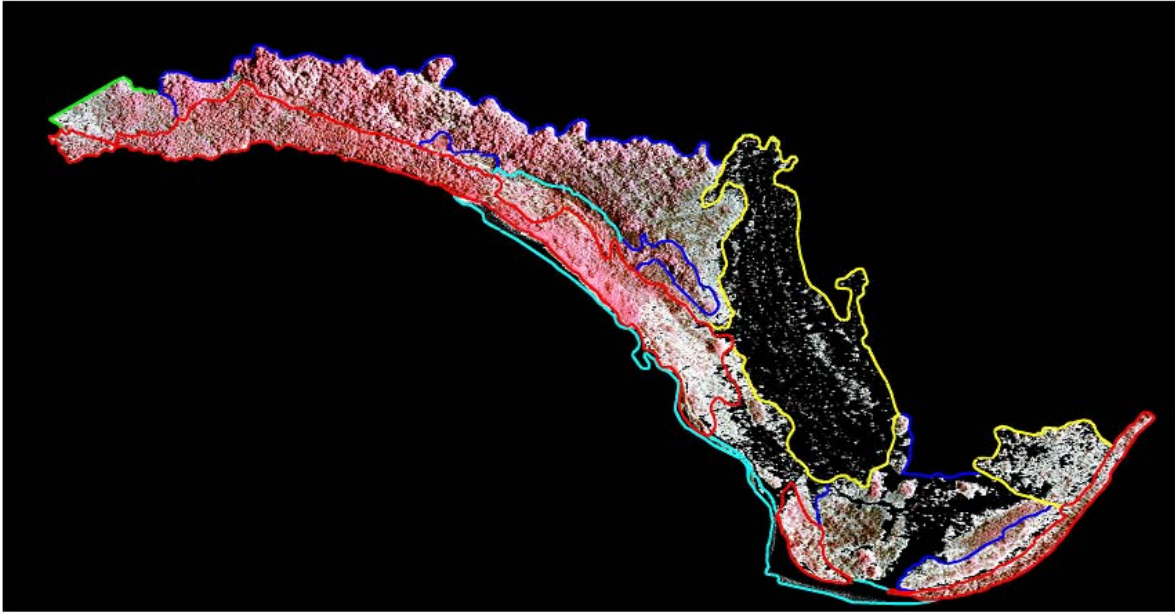


Figure 22. Vegetation unit outlines superposed on CIR image of study site RM68.2.

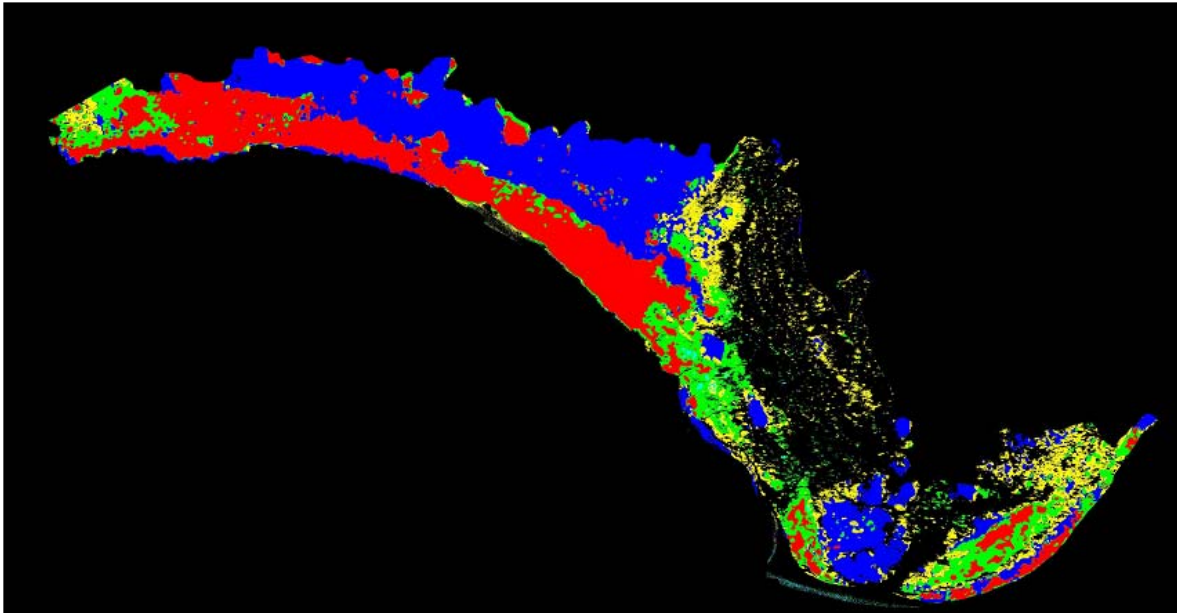


Figure 23. Vegetation classification map of study site RM68.2 produced using maximum likelihood classifier on July, 2000 11-cm CIR band data and texture data. Map excludes bare ground.

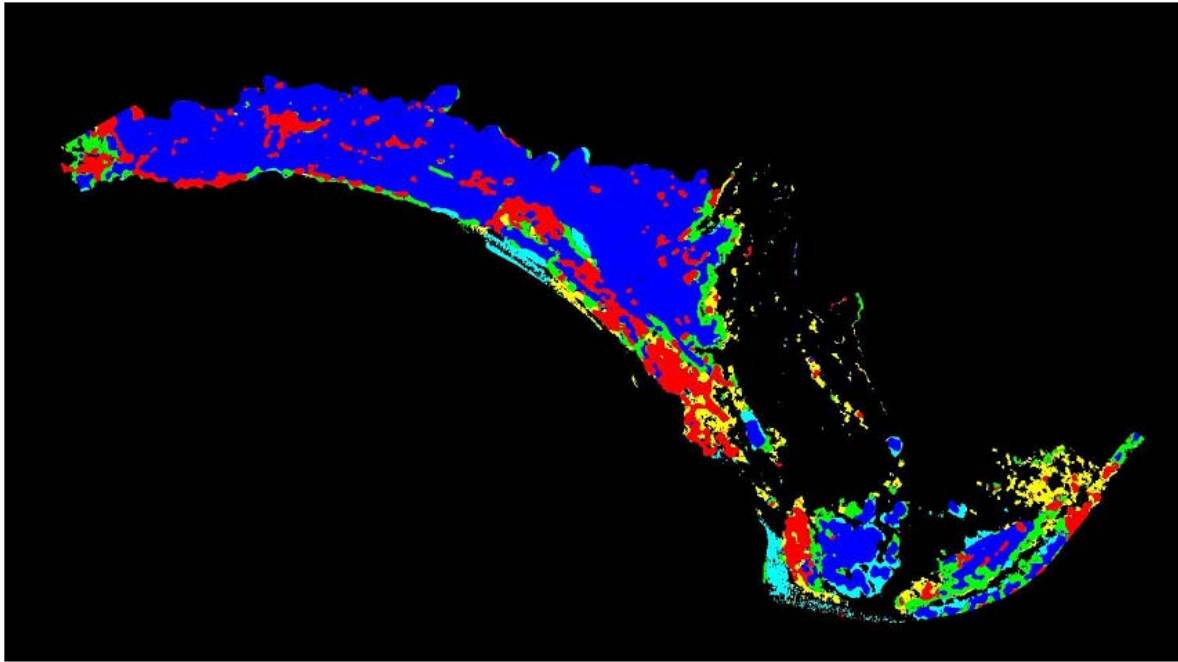


Figure 24. Vegetation classification map of study site RM68.2 produced using maximum likelihood classifier on March, 2000 30.5-cm CIR band data and texture data. Map excludes bare ground.

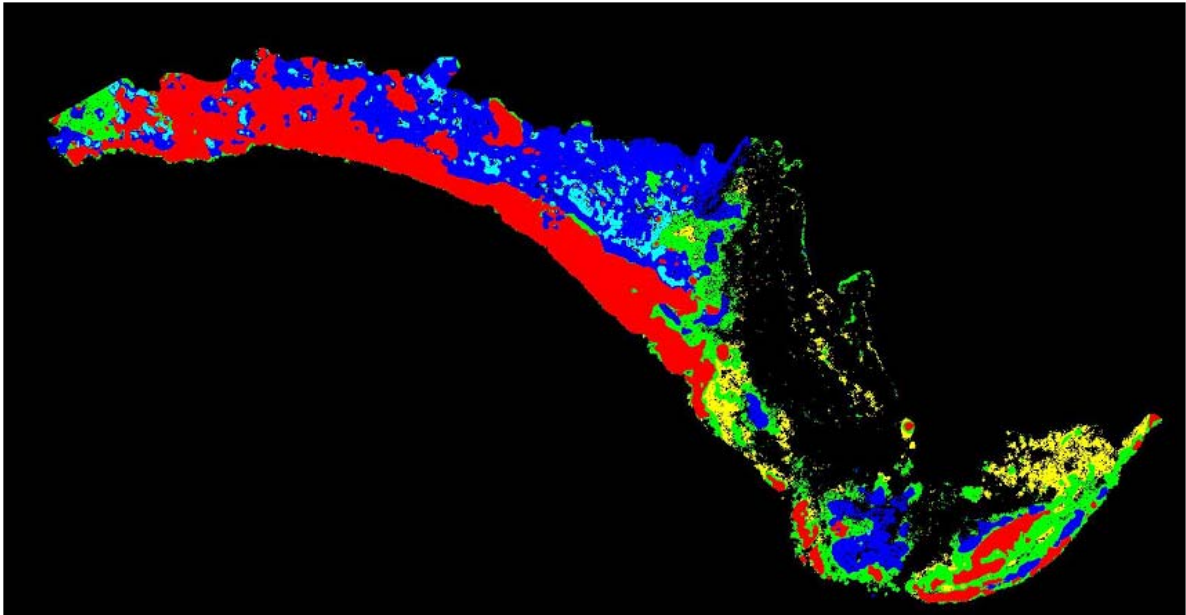


Figure 25. Vegetation classification map of study site RM68.2 produced using maximum likelihood classifier on September, 2000 28-cm CIR band data and texture data. Map excludes bare ground.

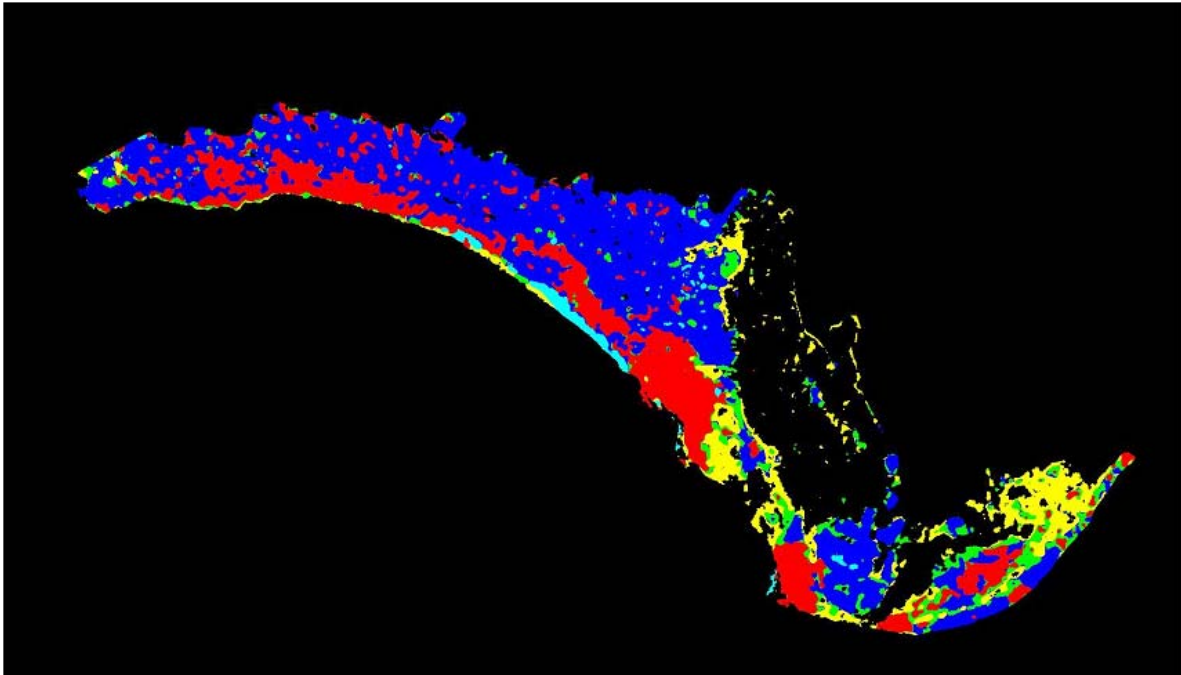


Figure 26. Vegetation classification map of study site RM68.2 produced using maximum likelihood classifier on September, 1999 30.5-cm Emerge CIR band data and texture data. Map excludes bare ground.

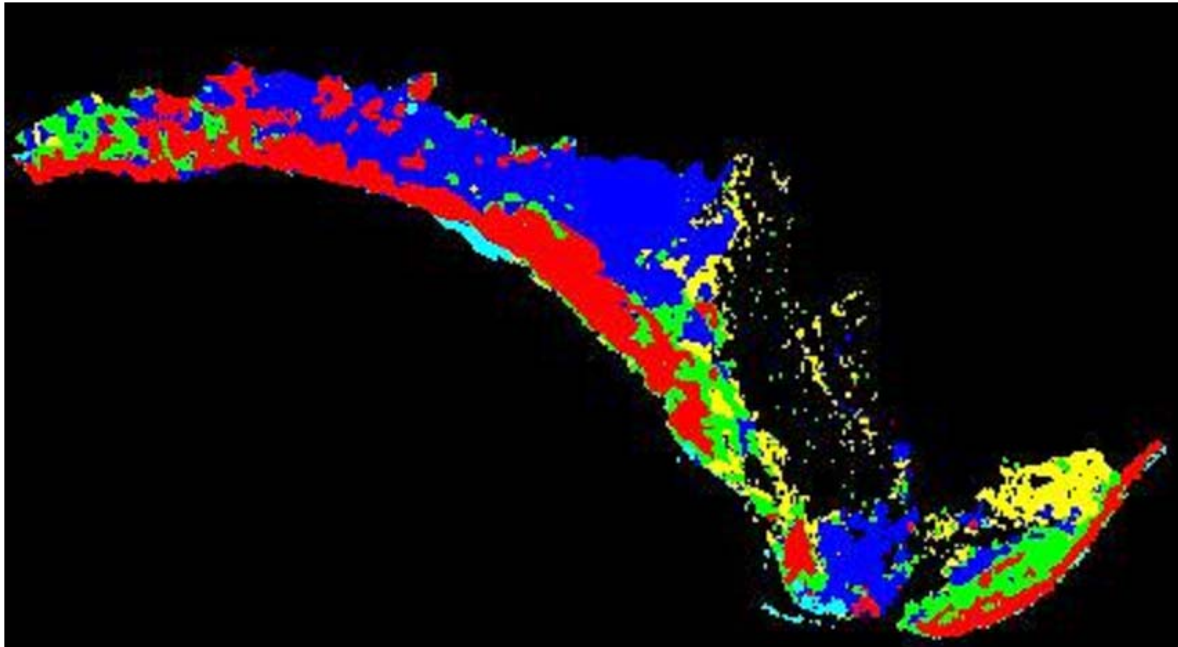


Figure 27. Vegetation classification map of study site RM68.2 produced using maximum likelihood classifier on July, 2000 100-cm ATM band data and texture data. Map excludes bare ground.

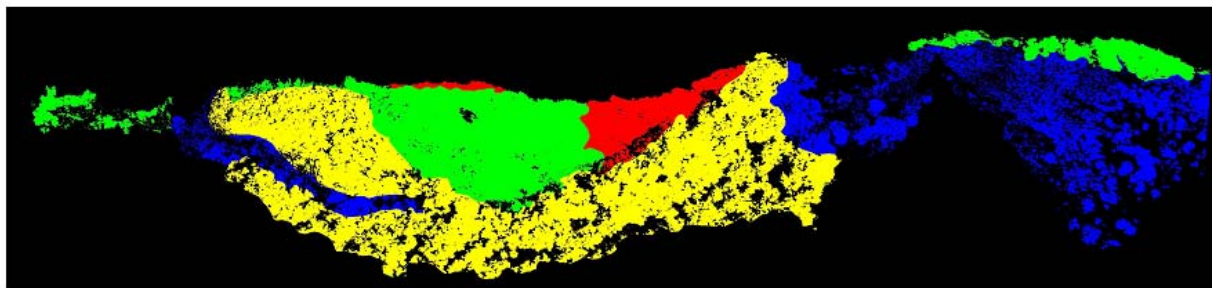


Figure 28. Vegetation map of study site RM71.4 produced from field observations by Kearsley and Ayers (2000). Map excludes bare ground.

	Vegetation Series	Vegetation Association
■	Phragmites	bulrush, rush
■	Coyote willow	baccharis, equisetum
■	Arrowweed	camel thorn, red brome
■	Goodding willow	tamarisk, red brome

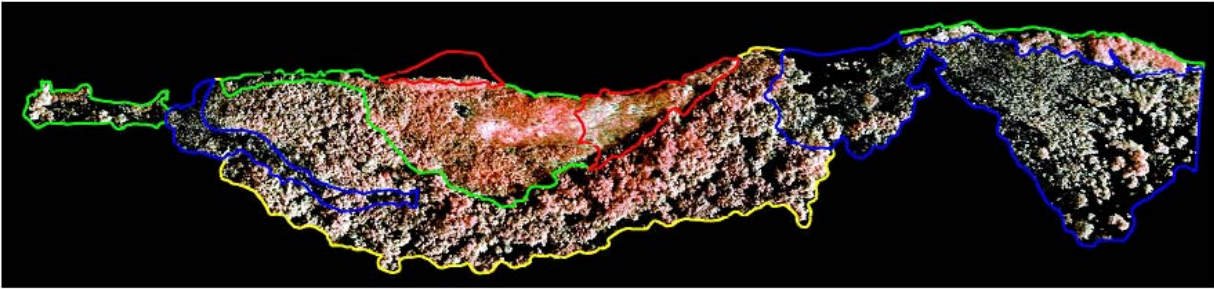


Figure 29. Vegetation unit outlines superposed on CIR image of study site RM71.4.

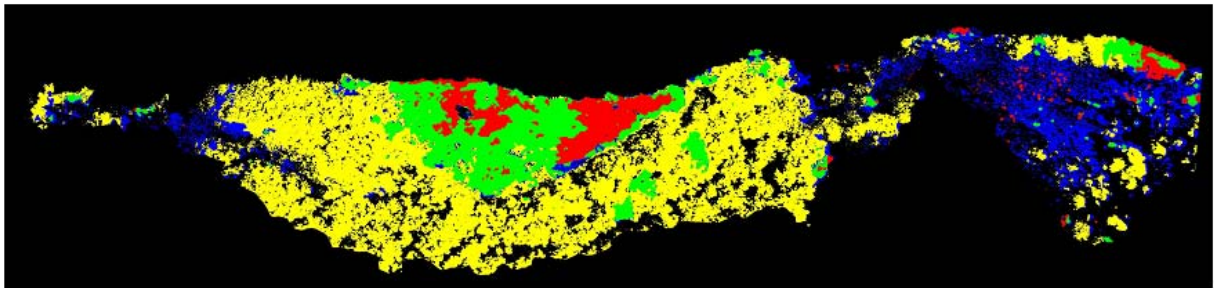


Figure 30. Vegetation classification map of study site RM71.4 produced using maximum likelihood classifier on July, 2000 11-cm CIR band data and texture data. Map excludes bare ground.

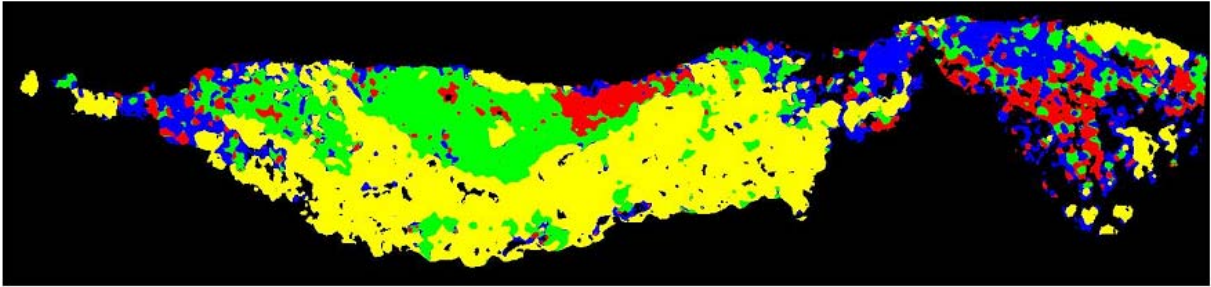


Figure 31. Vegetation classification map of study site RM71.4 produced using maximum likelihood classifier on September, 1999 30.5-cm Emerge CIR band data and texture data. Map excludes bare ground.

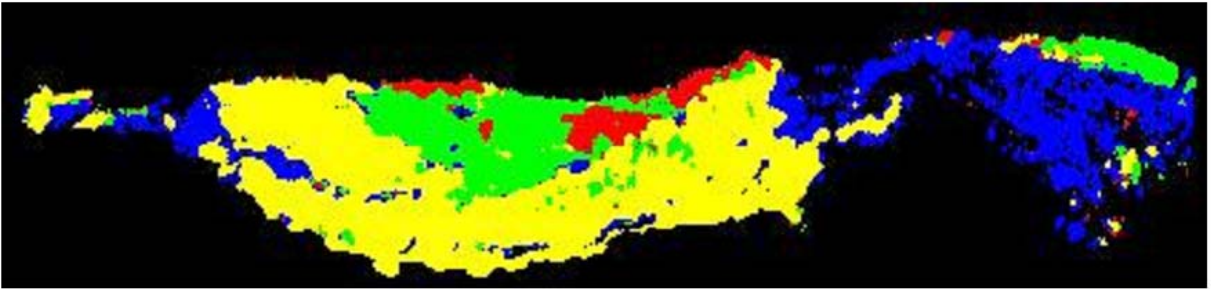


Figure 32. Vegetation classification map of study site RM71.4 produced using maximum likelihood classifier on July, 2000 100-cm ATM band data and texture data. Map excludes bare ground.

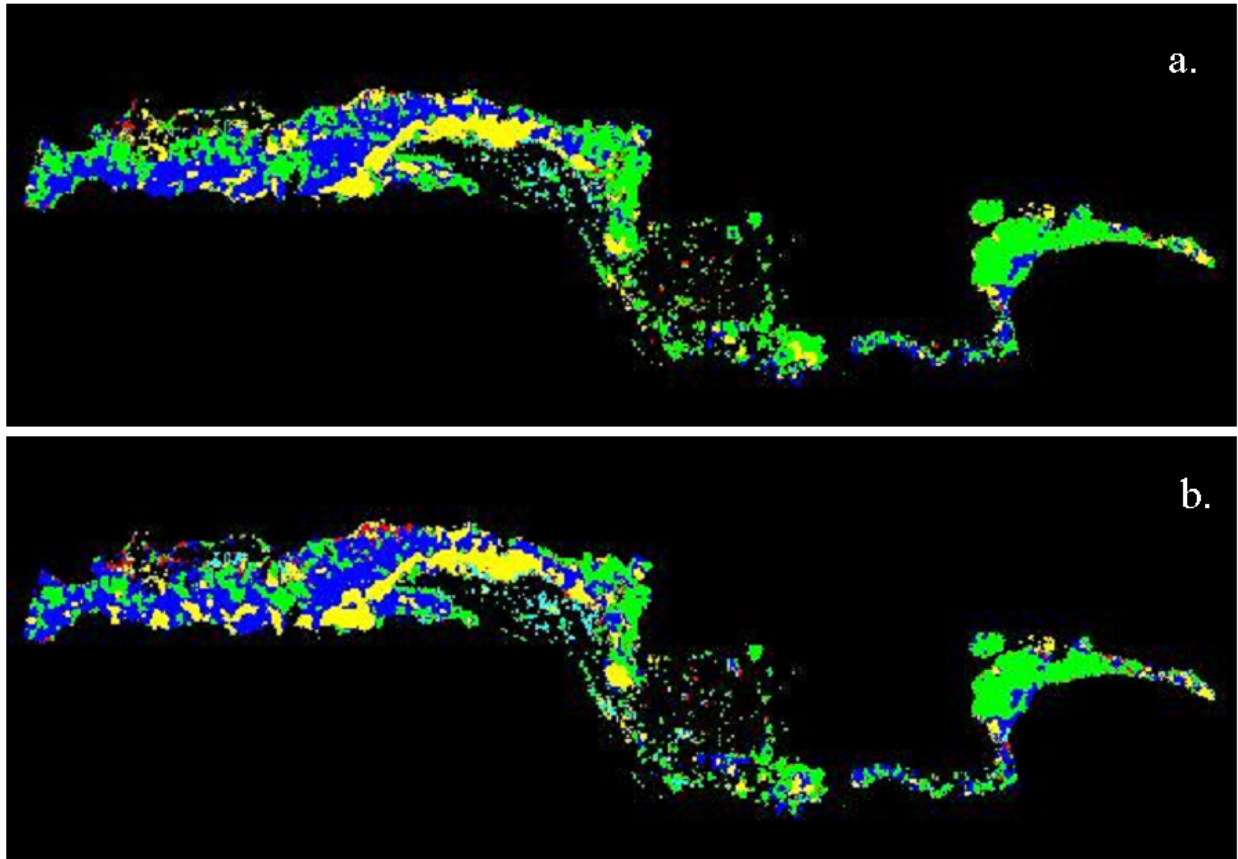


Figure 33. Comparison of vegetation classification maps of study site RM43.1 produced from maximum likelihood classification of July, 2000 100-cm ATM data using (a) texture and 8-band reflectance data versus (b) texture and 4-band reflectance. Map excludes bare ground.

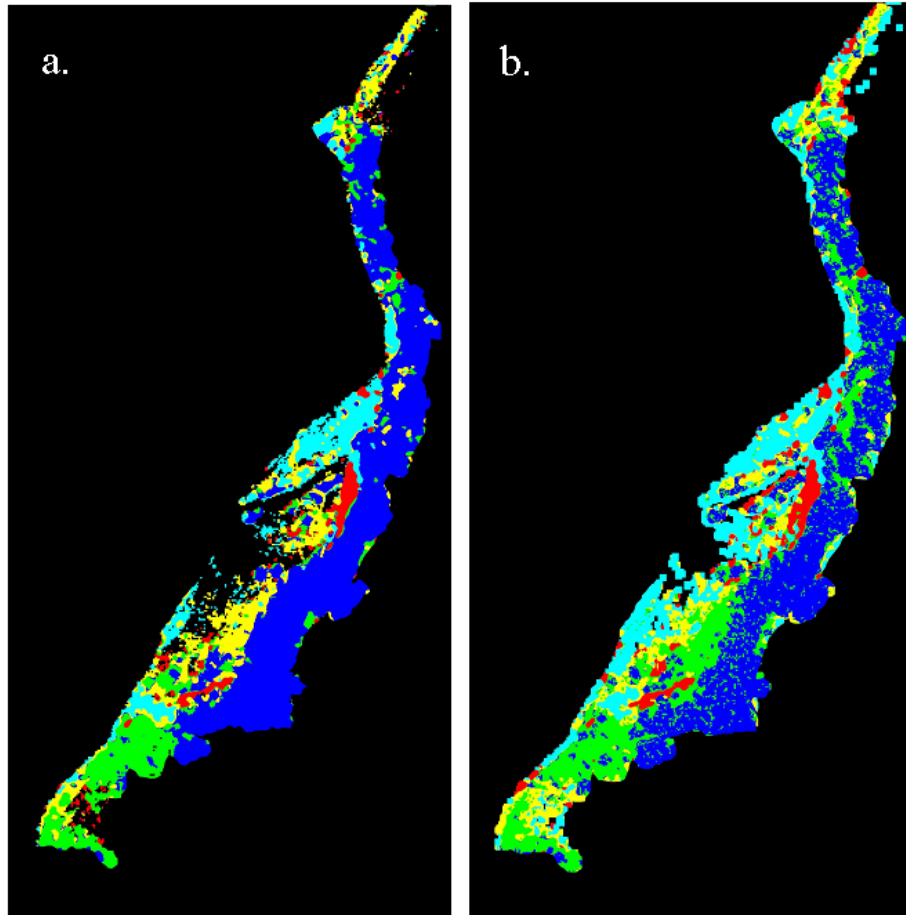


Figure 34. Comparison of vegetation classification maps of study site RM51 produced from maximum likelihood classification of July, 2000 100-cm ATM data using (a) texture and 8-band reflectance data versus (b) texture and 4-band reflectance. Map excludes bare ground.

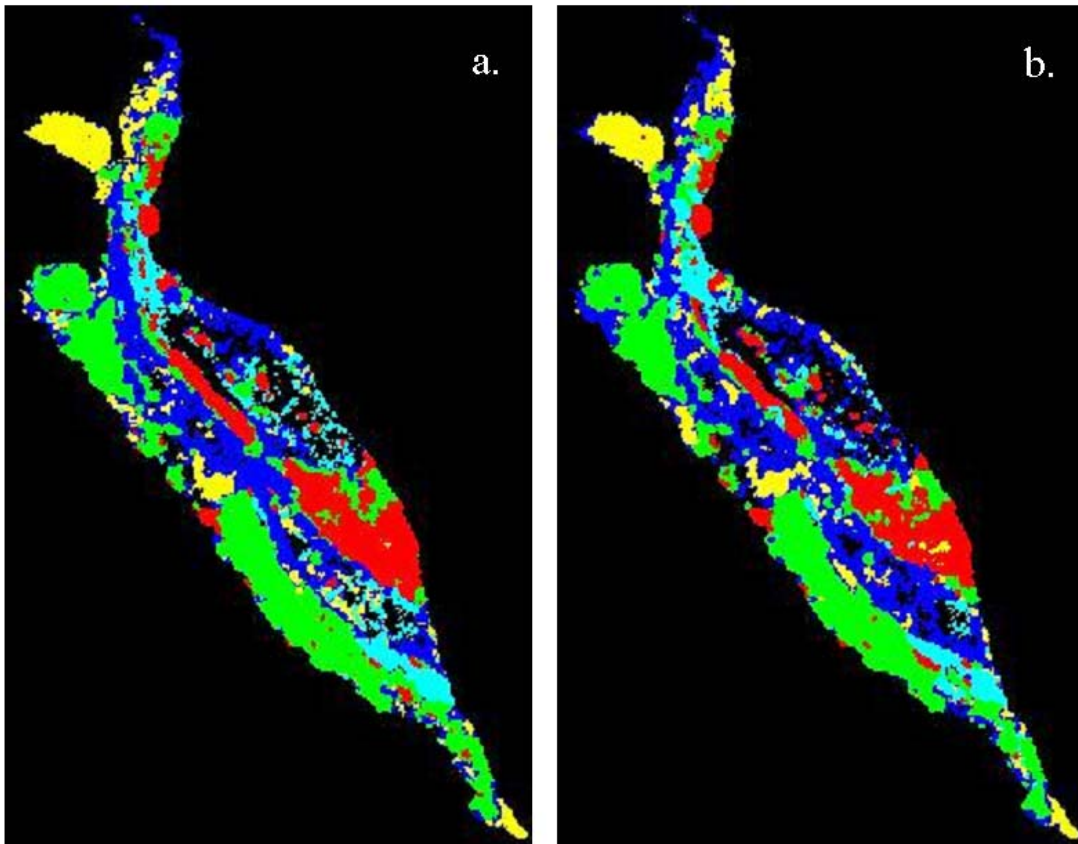


Figure 35. Comparison of vegetation classification maps of study site RM55.5 produced from maximum likelihood classification of July, 2000 100-cm ATM data using (a) texture and 8-band reflectance data versus (b) texture and 4-band reflectance. Map excludes bare ground.

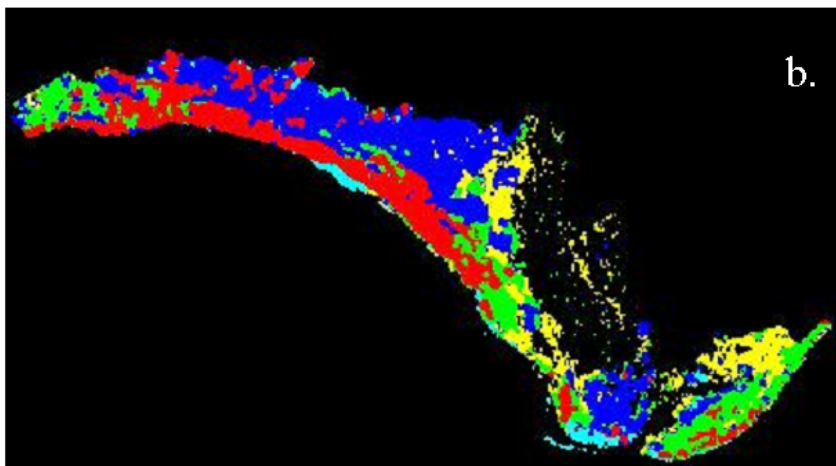
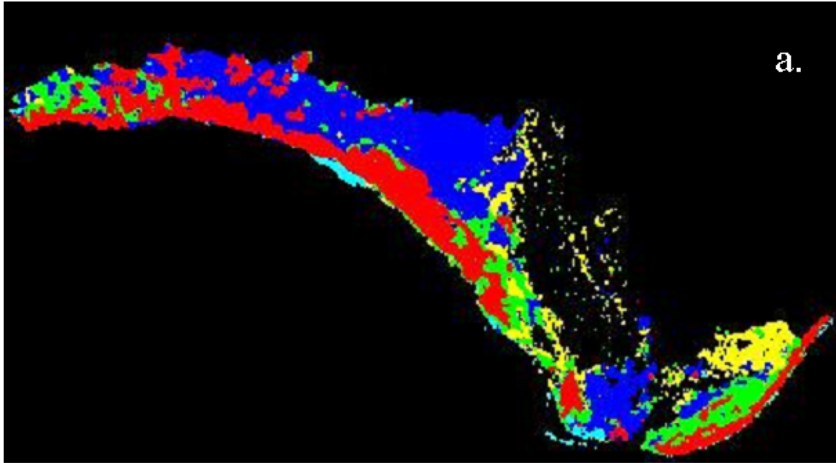


Figure 36. Comparison of vegetation classification maps of study site RM68.2 produced from maximum likelihood classification of July, 2000 100-cm ATM data using (a) texture and 8-band reflectance data versus (b) texture and 4-band reflectance. Map excludes bare ground.

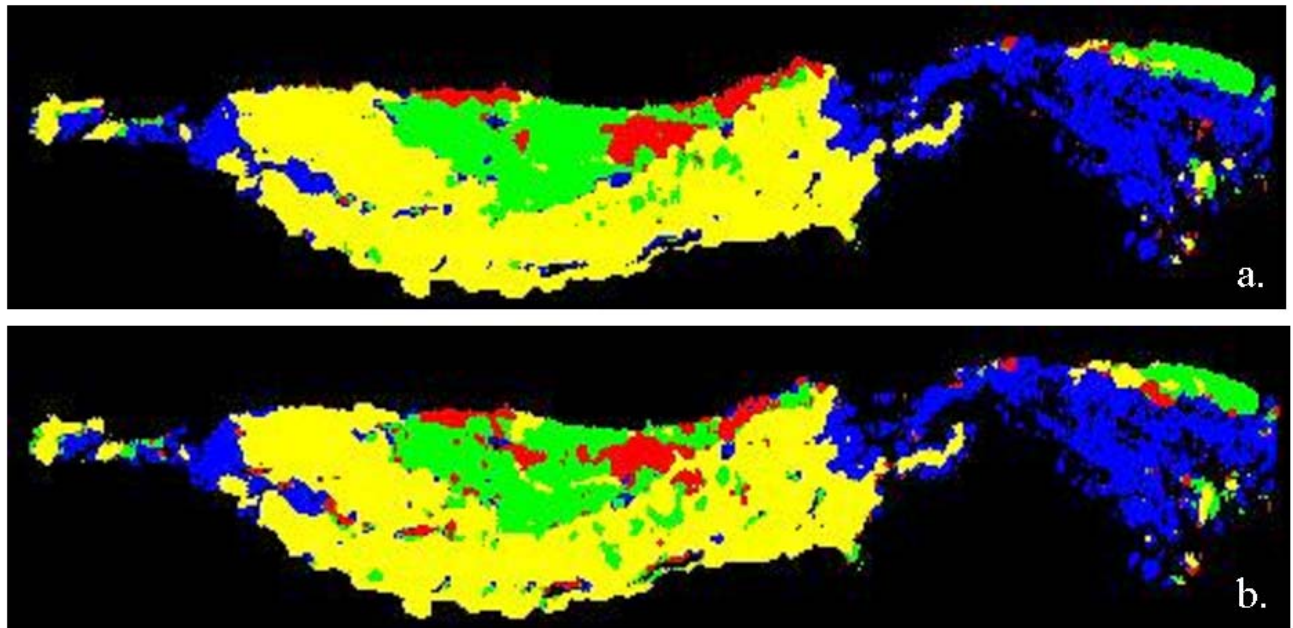


Figure 37. Comparison of vegetation classification maps of study site RM71.4 produced from maximum likelihood classification of July, 2000 100-cm ATM data using (a) texture and 8-band reflectance data versus (b) texture and 4-band reflectance. Map excludes bare ground.

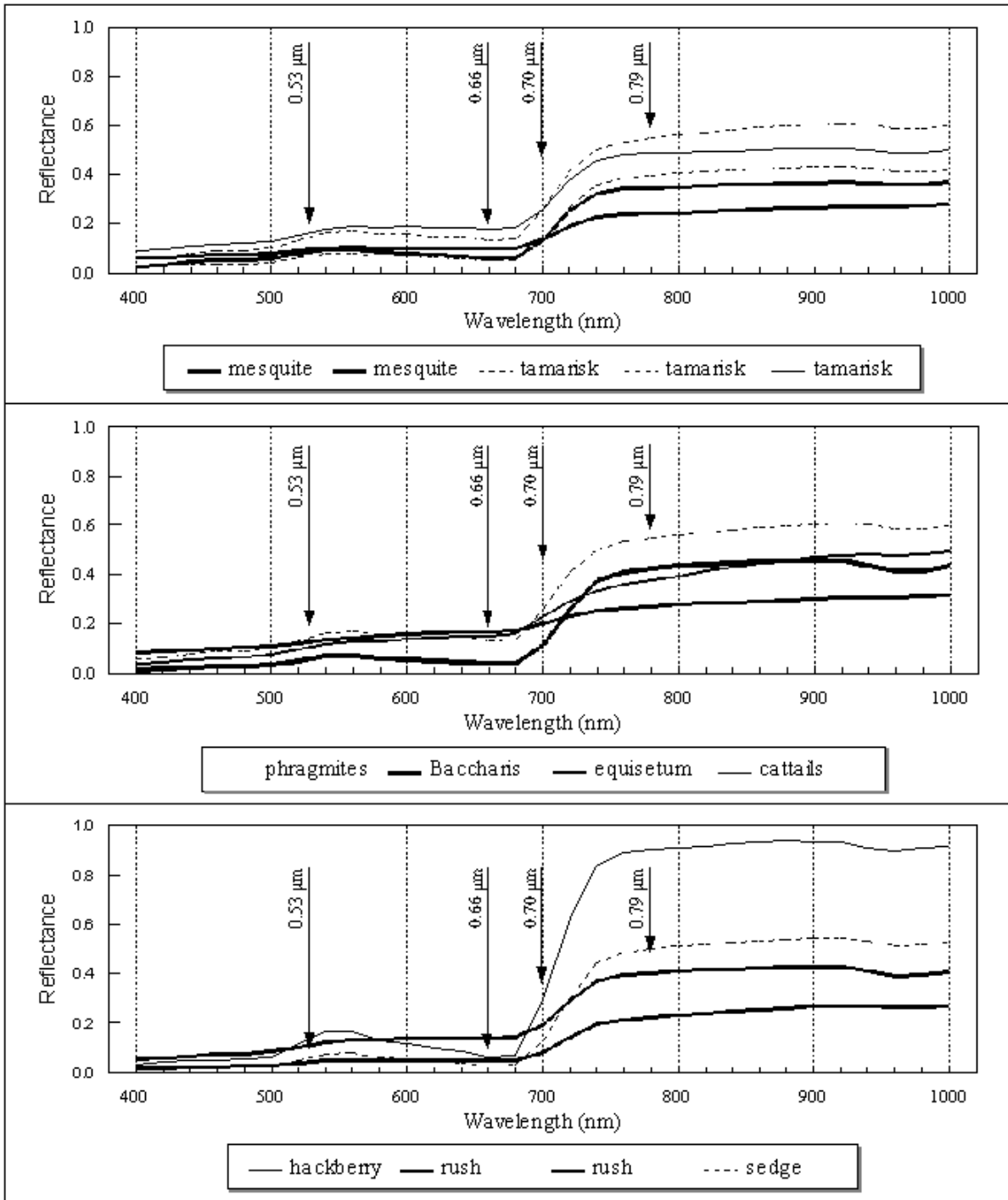


Figure 38. Locations of four optimum wavelength bands (indicated by arrows) within the 0.5-1.0 μm wavelength region for discriminating Grand Canyon riparian vegetation. Optimum band wavelengths derived from determinant analyses of field reflectance spectra of different riparian species, some of which are shown

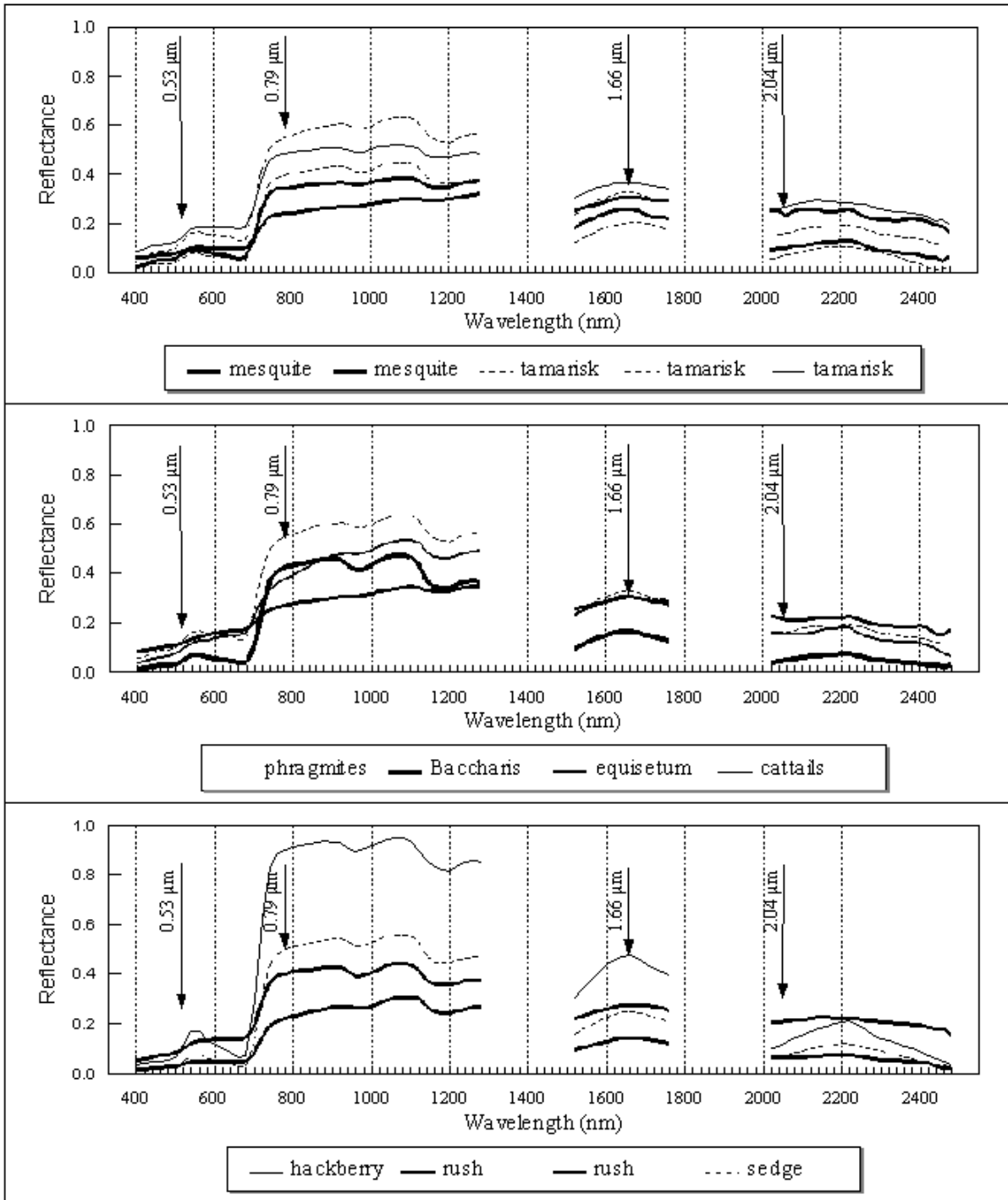


Figure 39. Locations of four optimum wavelength bands (indicated by arrows) within the 0.5-2.4 μm wavelength region for discriminating Grand Canyon riparian vegetation. Optimum band wavelengths derived from determinant analyses of field reflectance spectra of different riparian species, some of which are shown